Solar Sail Equilibria with Albedo Radiation Pressure in the Circular Restricted Three Body Problem

AE8900 MS Special Problems Report
Space Systems Design Lab (SSDL)
Guggenheim School of Aerospace Engineering
Georgia Institute of Technology
Atlanta, GA

Author:
Mariusz E. Grøtte

Advisor:
Marcus J. Holzinger

May 1, 2015

Solar Sail Equilibria with Albedo Radiation Pressure in the Circular Restricted Three Body Problem

Mariusz E. Grøtte[1]

Georgia Institute of Technology, 270 Ferst Drive Atlanta, GA 30332-0150, USA

Marcus J. Holzinger[2]

Georgia Institute of Technology, 270 Ferst Drive Atlanta, GA 30332-0150, USA

Abstract

In this paper the albedo radiation pressure (ARP) is investigated in the circular restricted three body problem (CR3BP) for a system consisting of the Sun, a minor body and a solar sail. The analytical framework is provided with extension to the solar radiation pressure (SRP) theory. The minor body is treated as Lambertian with bidirectional reflectance distribution function (BRDF) for approximation purposes. In this study it is found that ARP dominates SRP in a volume around the minor body which extends to L_1 and L_2, characterized as the region of influence (RoI) with an analytically defined boundary. Numerical simulations show that the inclusion of albedo effects generates new locations of artificial equilibrium points nearby the minor body, an important fact to address for solar sail missions to asteroids and comets. Local stability and controllability at equilibrium points are investigated and the system is found to be unstable but controllable in general when solar sail attitude angles are chosen as control inputs. Furthermore, equilibrium points along the RoI boundary are found to be Lyapunov stable.

Keywords: Restricted Three Body Problem; Solar Sail; Asteroids; Albedo Effects; Lambertian

Email addresses: msantora3@gatech.edu (Mariusz E. Grøtte), holzinger@gatech.edu (Marcus J. Holzinger)

[1]Graduate Student, School of Aerospace Engineering, Georgia Institute of Technology

[2]Assistant Professor, School of Aerospace Engineering, Georgia Institute of Technology

1. Introduction

Over the past decade space agencies worldwide have executed several missions to primitive bodies such as asteroids and comets. Increasing interest from the scientific communities in understanding their environment, value as promising mining-resource and role as indicators about the creation of the Solar System (Sonter, 1997; Nesvorny et al., 2003). In 2005 the Hayabusa mission, governed by Japan Aerospace Exploration Agency (JAXA), has provided more information about the dynamical environment of Asteroid 25143 Itokawa and samples from its surface (Scheeres et al., 2007; Michel and Yoshikawa, 2005). The Rosetta mission to the comet 67P/Churyumov-Gerasimenko performed a successful landing with its probe Philae on 12 November 2014 which returned important data about the surface (Taylor et al., 2015). Furthermore, in March 2015 the Dawn spacecraft arrived at the dwarf planet Ceres to look for habitable oceans and study the relationship between the asteroid belt and formation of the Solar System (Hand, 2015).

Solar sail propulsion is applicable to a wide range of missions. This spacecraft design provides the benifits of potential low-cost and long-term missions, controllable maneuvers at artificial Lagrange points, or equilibrium points, and are easily transferred to configurations such as Halo orbits around these equilibrium points, also named libration points (Farquhar and Kamel, 1973; Howell, 1984; McInnes et al., 1994; Farres and Jorba, 2012). Studies about solar sail dynamics around comets, where it is claimed that the sails may orbit the comet at Sun-side equilibrium points during its perihelion passage are discussed in Scheeres and Marzari (2002). Solar radiation pressure (SRP) and the strength of solar tides are claimed to alter the stability characteristics of the equilibrium points when in the vicinity of the Sun, inducing easily controlled orbits as discussed in Burns et al. (1979), in which the importance of SRP force exerted on smaller particles is emphasized. Ershkov (2012) provides a detailed analysis of a photogravitational restricted three body problem of a small particle system which can be theoretically linked to asteroids and their effects on the spacecraft from emitted radiation.

Control methods applicable for spacecraft hovering over Near-Earth Asteroids (NEAs) are discussed in Broschart and Scheeres (2005), which can ease the difficulty of orbiting small, irregularly sized and low-gravity objects. The body-fixed hovering behavior maintains the spacecraft relative position which can prove to be advantageous in acquiring close high-resolution images

of a particular surface. In fact, solar sails primarily utilize this hovering concept combined with change in attitude or sail area trim to alter the location of equilibrium points. McInnes et al. (1994) studies the available libration points for solar sails in CR3BP that are Lyapunov unstable, but establishes that they are in general controllable using sail attitude feedback control alone. In general, it is claimed that the sailing capability offers potential low-cost missions and flexible methods for exploring the solar system (Macdonald and McInnes, 2011). In a conceptual and simplified version of the solar sail, when modeled as a perfectly reflecting flat plate, these equilibrium points depend on sail attitude and strength of SRP and gravity forces. Morrow et al. (2001) further investigates the solar sail CR3BP dynamics with Hill approximation, a mathematical tool which applies well to the motion of spacecraft around asteroids. In the paper it is confirmed that the sail acceleration renders restrictions when hovering over or orbiting smaller bodies due to inevitable sensitivities to the perturbations being present.

To establish an analytical framework to incorporate SRP into the equations of motion (EoM), the initial steps are to investigate the CR3BP with SRP in a Sun-minor body system. Solar sails are inherently sensitive to photons it is proposed in this paper to investigate the additional effects from the smaller body albedo, or albedo radiation pressure (ARP). Emphasis is made on ARP as a significant force in addition to SRP in CR3BP and new conditions are identified. The minor body is modeled as a Lambertian diffuse gray body with its albedo effects modeled by means of optical signature magnitude based on the relative distance to viewer i.e. solar sail. The albedo scattering is determined by the bidirectional reflectance distribution function (BRDF). Since the dynamics will alter in vicinity of minor body, it is important to investigate local stability and controllability at the equilibrium points. Due to high number of degrees of freedom, local stability is best analyzed through applying the method of Routh-Hurwitz criterion (McInnes, 1999). Controllability is established conventionally through analyzing the controllability matrix with control inputs chosen to be the solar sail pitch and precession angles, claimed to be good choices together with sail area trimming (Hexi and McInnes, 2005).

The contributions in this paper are listed as follows: (a) equilibrium surfaces as a function of solar sail lightness number in a Sun-asteroid CR3BP system with both SRP and ARP, (b) extension of existing constraints identifying regions of where equilibrium solutions exist, (c) regions of where SRP or ARP forces are balanced or separately dominant are analytically identi-

fied and (d) local stability and controllability at the equilibrium points are analyzed.

This paper is organized as follows. Section 2 describes the background of the material and provides the literature review up to date. The equations presented here serve as basis for further discussion and include only SRP in the EoM. Section 3 describes the means necessary for an adequate approximation of including ARP in the CR3BP system. Method of incorporating albedo effects, the force model and conditions for equilibrium solutions are modified. Extension to the existing constraints and region of influence are shown analytically. Section 4 discusses the stability and control of the solar sail at the equilibrium points. Linearization about local nonlinear dynamics is favored over linearization about trajectories since there are no new fundamental findings based on the local time-varying dynamics. Discussion about whether the solar sail is controllable or not is presented here. Results are given in Section 5 and validates the analytically defined framework and shows how equilibrium points vary based on both SRP and ARP for selected parametrization of solar sail lightness number. Conclusions are given in section 6 and summarizes the findings and what impacts this may have on current and future missions. In Appendix A a more rigorous discussion of the background material is presented with influence from the notation in McInnes et al. (1994); McInnes (1999). Appendix B-Appendix F show the partial derivatives used in section 4 to analyze stability and controllability. Appendix G provides the correct derivation of previous erroneously defined partial derivatives in McInnes (2000).

2. Theory

The dynamics of a solar sail in the CR3BP with SRP have previously been established in McInnes et al. (1994); McInnes (1999) and serve as a model that is to be extended in this paper. The following results are briefly summarized here to serve as a foundation for the contributions in this work. More complete derivations are given in in Appendix A. The rotating $\mathcal{B}$ frame rotates once with angular velocity $\boldsymbol{\omega}_{\mathcal{B}/\mathcal{I}}$ about the $\hat{\mathbf{z}}$-axis or as seen by the inertial frame $\mathcal{I}$ in $2\pi/\omega$ time units. In this paper the dynamics are considered to be in the rotating $\mathcal{B}$ frame unless otherwise stated, thus the notation for the frames will be dropped further on. The dimensions are normalized such that the distance between the primary masses r_{12}, the sum of primary masses $m_1 + m_2$, angular velocity magnitude $\|\boldsymbol{\omega}_{\mathcal{B}/\mathcal{I}}\|_2$ and the gravitational constant

G are all defined to be unity. The mass ratio of the system is defined as $\mu = m_2/(m_1 + m_2)$. Fig. 1 shows the geometry of the CR3BP system in the rotating reference frame, where all units are nondimensionalized.

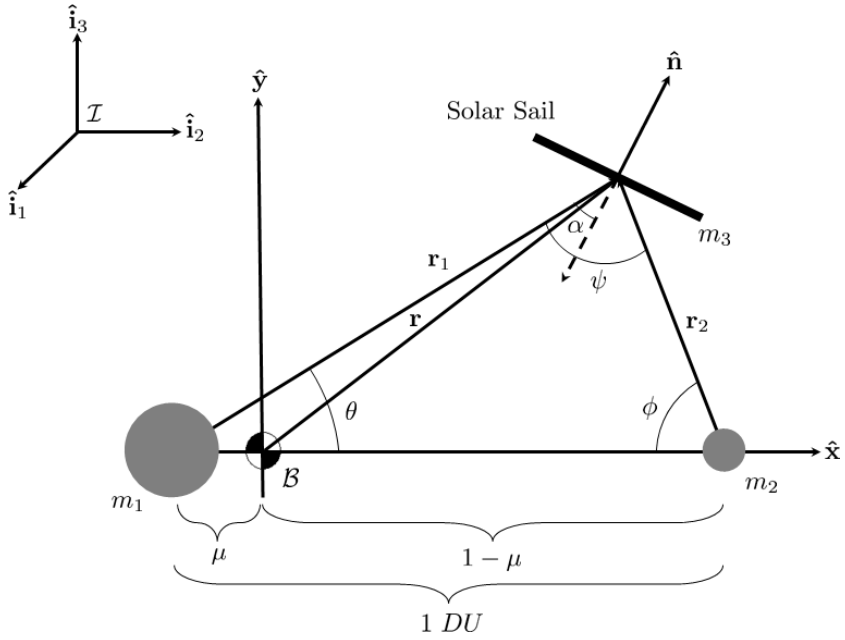

Figure 1: Schematic geometry of the solar sail restricted three body problem in the $\hat{\mathbf{x}} - \hat{\mathbf{y}}$ rotating frame.

The reduced vector form of equations of motion (EoM) for a solar sail with $\mathbf{r}$ being the vector from the center of mass to m_3 may be defined in the rotating frame as shown in McInnes et al. (1994)

$$\ddot{\mathbf{r}} + 2\boldsymbol{\omega} \times \dot{\mathbf{r}} + \boldsymbol{\nabla} U = \mathbf{a}_1 \tag{1}$$

When the solar sail is in equilibrium between gravitational and SRP accelerations, the state space form describing the EoM may be written as

$$\dot{\mathbf{x}} = \begin{bmatrix} \dot{\mathbf{r}} \\ \ddot{\mathbf{r}} \end{bmatrix} = \mathbf{0}_{6\times 1} = \begin{bmatrix} \mathbf{0}_{3\times 1} \\ \mathbf{a}_1 - \boldsymbol{\nabla} U \end{bmatrix}_{6\times 1} \tag{2}$$

The SRP acceleration of a solar sail in CR3BP may be written as

$$\mathbf{a}_1 = \beta \frac{(1-\mu)}{r_1^2} \langle \hat{\mathbf{r}}_1 \cdot \hat{\mathbf{n}} \rangle^2 \hat{\mathbf{n}} \tag{3}$$

Knowing that $\hat{\mathbf{r}}_1$ is directed along the Sun-line and since the SRP force can never be directed sunwards, the solar sail acceleration is constrained (McInnes et al., 1994). Therefore the $\langle \cdot \rangle$ term is defined as the nonnegative operator i.e.

$$\langle x \rangle = \begin{cases} x & \text{if } x \geq 0 \\ 0 & \text{if } x < 0 \end{cases}$$

The solar sail lightness number β is an important design parameter which defines the ratio of SRP acceleration to gravitational acceleration. β is defined as

$$\beta = \frac{\sigma^*}{\sigma} \tag{4}$$

where

$$\sigma^* = \frac{\mathfrak{L}_1}{2\pi G m_1 c} \tag{5}$$

where $\mathfrak{L}_1$ is the luminosity of the large primary object, where for the Sun it is taken to be approximately $3.846 \times 10^{26}\ W$. It can be seen that a large β is induced by larger $\frac{1}{\sigma} = A/m_3$ i.e. the sail acceleration $\mathbf{a}_1$ is proportional to the sail area and inversely proportional to the spacecraft mass. However it will also be shown that acceleration $\mathbf{a}_1$ is also highly dependent on the sail orientation as indicated by the nonnegative operator $\langle \cdot \rangle$. For comparison and building intuition, Table 1 shows different values of β for spacecraft that have been tested and deployed in space. Typically values of $\beta = 0.001 - 0.3$ are feasible (McInnes, 1999). It is to be noted that the examples are not treated as perfect solar sails with 100 % specular reflection.

Table 1: Solar sail lightness numbers for relevant spacecraft

Spacecraft	β
GeoStorm (McInnes, 1999)	0.02
Interstellar Heliopause Probe (McInnes, 1999)	$0.3 - 0.6$
IKAROS (Tsuda et al., 2013)	0.001
Sunjammer (Heiligers and McInnes, 2014)	$0.0388 - 0.0445$

At equilibrium, where SRP and gravitational accelerations are balanced, the sail normal vector $\hat{\mathbf{n}}$ can defined as the unit vector of the gradient of pseudo-potential

$$\hat{\mathbf{n}} = \frac{\boldsymbol{\nabla} U}{\|\boldsymbol{\nabla} U\|_2} \tag{6}$$

The solar sail orientation angles, pitch (cone) and precession (clock) angles in order, can also be expressed at equilibrium as the following

$$\tan\alpha = \frac{\|\hat{\mathbf{r}}_1 \times \boldsymbol{\nabla} U\|_2}{\hat{\mathbf{r}}_1 \cdot \boldsymbol{\nabla} U} \tag{7}$$

$$\tan\gamma = \frac{\|((\hat{\mathbf{r}}_1 \times \hat{\mathbf{z}}) \times \hat{\mathbf{r}}_1) \times (\hat{\mathbf{r}}_1 \times \boldsymbol{\nabla} U)\|_2}{((\hat{\mathbf{r}}_1 \times \hat{\mathbf{z}}) \times \hat{\mathbf{r}}_1) \cdot (\hat{\mathbf{r}}_1 \times \boldsymbol{\nabla} U)} \tag{8}$$

As indicated on Fig. 1 an additional sail orientation angle has to be defined with respect to $\mathbf{r}_2$ and can be defined as

$$\tan(\psi - \alpha) = \frac{(\|\hat{\mathbf{r}}_1 \times \hat{\mathbf{r}}_2\|_2)(\hat{\mathbf{r}}_1 \cdot \boldsymbol{\nabla} U) - (\hat{\mathbf{r}}_1 \cdot \hat{\mathbf{r}}_2)(\|\hat{\mathbf{r}}_1 \times \boldsymbol{\nabla} U\|_2)}{(\hat{\mathbf{r}}_1 \cdot \hat{\mathbf{r}}_2)(\hat{\mathbf{r}}_1 \cdot \boldsymbol{\nabla} U) + (\|\hat{\mathbf{r}}_1 \times \hat{\mathbf{r}}_2\|_2)(\|\hat{\mathbf{r}}_1 \times \boldsymbol{\nabla} U\|_2)} \tag{9}$$

At an equilibrium point the solar sail lightness number β may be found from the following expression

$$\beta = \frac{r_1^2}{(1-\mu)} \frac{\boldsymbol{\nabla} U \cdot \hat{\mathbf{n}}}{\langle \hat{\mathbf{r}}_1 \cdot \hat{\mathbf{n}} \rangle^2} \tag{10}$$

By evaluating the nonnegative operator $\langle \hat{\mathbf{r}}_1 \cdot \hat{\mathbf{n}} \rangle$, a boundary $S(\mathbf{r}_1, \mathbf{r}_2) = 0$ can be found when $\hat{\mathbf{r}}_1 \cdot \hat{\mathbf{n}} = 0$ as shown in McInnes et al. (1994). The condition exists when SRP has no effect on the solar sail i.e. when the sail is oriented at $|\alpha| = 90^\circ$ or more intuitively when $\beta \to \infty$. The boundary is written as

$$S(\mathbf{r}_1, \mathbf{r}_2) = x(x+\mu) + y^2 - \frac{1-\mu}{r_1} - \mu \frac{\mathbf{r}_1 \cdot \mathbf{r}_2}{r_2^3} \tag{11}$$

and defines possible locations for equilibria in CR3BP in the rotating reference frame. The boundary exists in form of two topologically disconnected surfaces and separates regions where equilibrium solutions may and may not exist as shown in previous work (McInnes et al., 1994). In the free areas the equilibrium points indicate that the solar sail is in tension between SRP and gravitational forces.

Based on the methodology described here and in McInnes (1999), the following section will include the ARP force in CR3BP solar sail dynamics and generate equivalent analytical results for acceleration terms, conditions and new boundaries.

3. Inclusion of Albedo Effects

Based on the EoM in CR3BP with SRP effects given in Eq. (1), the model is now extended to include the ARP. As an approximation, luminosity of the body is characterized by the bidirectional reflectance distribution function (BRDF) and is therefore treated as an Lambertian diffuse model. It is known that for Lambertian BRDF, the reflecting radiation can be expressed as a function of the angle between the Sun-line vector $\hat{\mathbf{r}}_{12}$ with respect to the body m_2 and the viewer line of sight $\hat{\mathbf{r}}_2$ (Magnusson et al., 1996; Kaasalainen et al., 2002). Several techniques have been developed to estimate albedo values. A reasonable reflectance number for asteroids should be approximately $\rho = 0.1 - 0.2$ (Fernandez et al., 2005; Busch et al., 2008). Asteroids are treated as gray bodies such that ρ is constant for all wavelengths but with low emissivity, which is consistent with some of the previous studies found in Krag (1974). Furthermore the technique of optical signatures have frequently used the visual magnitude system, adopted from the astronomers. This method will also be applied here and serves as an approximation tool that may be extended in further study.

The optical signature magnitude of an asteroid M_2, when approximated as a sphere, is given by

$$M_2 = M_1 - 2.5 \log \left(\frac{d_2^2}{r_2^2} \rho p(\phi) \right) \tag{12}$$

where d_2 is the diameter of the asteroid and r_2 is the distance between the asteroid and the observing spacecraft. M_1 is the reference magnitude, taken here to be the Sun, and has the visual magnitude of -26.78 from the Earth with atmospheric effects being uncorrected (Krag, 1974; Shell, 2010). The Lambertian BRDF may be expressed in terms of a function of $\rho p(\phi)$ where ρ is albedo reflectance and $p(\phi)$ is the diffuse phase angle function as identified in Krag (1974). $p(\phi)$ is defined for a diffuse sphere as

$$p(\phi) = \frac{2}{3\pi^2} (\sin \phi + (\pi - \phi) \cos \phi) \tag{13}$$

For a fixed diameter d_2 and albedo ρ of the body m_2 and varying ϕ and r_2, represented here as $D(\phi; r_2, \rho, d_2)$, is obtained from rearranging Eq. (10) and is of the form

$$D(\phi; r_2, \rho, d_2) = \frac{d_2^2}{r_2^2} \rho p(\phi) \tag{14}$$

This term appears in the logarithm term in Eq. (12) with values ranging between $0 < D(\phi; r_2, \rho, d_2) < 1$ since the magnitude M_2 is restricted to be $M_2 \leq M_1$. More intuitively, this represents the ratio of luminosities of m_2 and m_1 as seen by the solar sail. Therefore the apparent luminosity of m_2, $\mathfrak{L}_2$, can be defined in terms of the luminosity of m_1, $\mathfrak{L}_1$, as

$$\mathfrak{L}_2(\phi; r_2, \rho, d_2) = \mathfrak{L}_1 D(\phi; r_2, \rho, d_2) \tag{15}$$

Having established the basic definitions for albedo, it is now possible to look at the additional force experienced on the solar sail due to ARP.

3.1. New Dynamics and Equilibrium Solutions

The total force exerted on the solar sail is expressed as

$$\sum \mathbf{F} = \mathbf{F}_g + \mathbf{F}_{SRP} + \mathbf{F}_{ARP} + \mathbf{F}_{other} \tag{16}$$

if $\mathbf{F}_{other}$ is neglected, then forces due to gravity $\mathbf{F}_g$, $\mathbf{F}_{SRP}$ and $\mathbf{F}_{ARP}$ are then considered. Definitions of SRP are given in Appendix A, where SRP and solar energy flux are defined as P_{SRP} and W_{SRP}, respectively. The expression for ARP magnitude is as follows

$$P_{ARP} = \frac{W_{ARP}}{c} \tag{17}$$

where c is the speed of light and W_{ARP} represents the energy flux of the electromagnetic albedo radiation from the asteroid that creates pressure on the solar sail. Assuming the Sun and the object are now treated as a luminous sources, the energy flux varies proportionally with the inverse square of the distance $\hat{\mathbf{r}}_{12}$ between the Sun and the body m_2. The albedo energy flux W_{ARP} can be written in terms of the asteroid luminosity $\mathfrak{L}_2(\phi; r_2, \rho, d_2)$ and scaled by the Sun-Earth distance R_E as

$$W_{ARP} = \frac{\mathfrak{L}_2(\phi; r_2, \rho, d_2)}{4\pi r_2^2} \tag{18}$$

Albedo photons from the second primary mass are reflected on solar sail, creating an additional force to $\mathbf{F}_{SRP}$. Incident directions of the photons from the Sun and m_2 are defined as $\hat{\mathbf{u}}_i$ and $\hat{\mathbf{v}}_i$, respectively. Specular reflected directions of the photons from the Sun and m_2 are defined as $\hat{\mathbf{u}}_r$ and $\hat{\mathbf{v}}_r$, respectively. The schematic of forces working on the perfectly reflecting

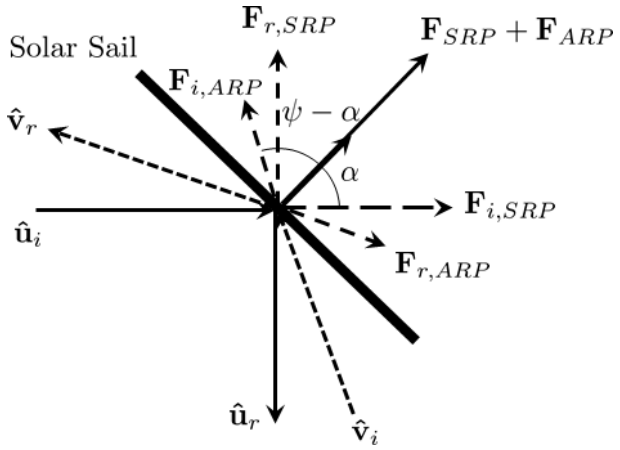

Figure 2: SRP and ARP forces exerted on a perfectly reflecting solar sail

solar sail is shown in Fig. 2. For a sail area A with unit vector $\hat{\mathbf{n}}$ in direction normal to the sail surface, the total force exerted on the sail due to photons incident from $\hat{\mathbf{u}}_i$ and $\hat{\mathbf{v}}_i$ directions is given by

$$\mathbf{F}_{i,SRP}+\mathbf{F}_{i,ARP}=P_{SRP}A(\hat{\mathbf{u}}_i\cdot\hat{\mathbf{n}})\hat{\mathbf{u}}_i+\tilde{P}A(\hat{\mathbf{v}}_i\cdot\hat{\mathbf{n}})\hat{\mathbf{v}}_i \tag{19}$$

where $A(\hat{\mathbf{u}}_i\cdot\hat{\mathbf{n}})$ and $A(\hat{\mathbf{v}}_i\cdot\hat{\mathbf{n}})$ are the projected sail areas in $\hat{\mathbf{u}}_i$ and $\hat{\mathbf{v}}_i$ directions, respectively. By Newton's Third Law, the reflected photons will exert a force of equal magnitude on the solar sail in the specular reflected direction $-\hat{\mathbf{u}}_r$ and $-\hat{\mathbf{v}}_r$, i.e.

$$\mathbf{F}_{i,SRP}+\mathbf{F}_{i,ARP}=-PA(\hat{\mathbf{u}}_i\cdot\hat{\mathbf{n}})\hat{\mathbf{u}}_r-\tilde{P}A(\hat{\mathbf{v}}_i\cdot\hat{\mathbf{n}})\hat{\mathbf{v}}_r \tag{20}$$

Since $\hat{\mathbf{u}}_i-\hat{\mathbf{u}}_r=2(\hat{\mathbf{u}}_i\cdot\hat{\mathbf{n}})\hat{\mathbf{n}}$ and $\hat{\mathbf{v}}_i-\hat{\mathbf{v}}_r=2(\hat{\mathbf{v}}_i\cdot\hat{\mathbf{n}})\hat{\mathbf{n}}$, the net photon force is then given by

$$\mathbf{F}_{i,SRP}+\mathbf{F}_{i,ARP}=2PA(\hat{\mathbf{u}}_i\cdot\hat{\mathbf{n}})^2\hat{\mathbf{n}}+2\tilde{P}A(\hat{\mathbf{v}}_i\cdot\hat{\mathbf{n}})^2\hat{\mathbf{n}} \tag{21}$$

Using Eq. (17) then Eq. (21) may be expressed as

$$\mathbf{F}_{SRP}+\mathbf{F}_{ARP}=\frac{2WA}{c}(\hat{\mathbf{u}}_i\cdot\hat{\mathbf{n}})^2\hat{\mathbf{n}}+\frac{2\tilde{W}A}{c}(\hat{\mathbf{v}}_i\cdot\hat{\mathbf{n}})^2\hat{\mathbf{n}} \tag{22}$$

The sail surface may experience SRP and ARP forces exerted on same side simultaneously or opposite sides exclusively, with respect to $\hat{\mathbf{n}}$, then Eq. (22)

needs to be redefined as

$$\mathbf{F}_{SRP}+\mathbf{F}_{ARP} = \frac{2WA}{c}(\hat{\mathbf{u}}_i\cdot\hat{\mathbf{n}})^2\,\mathrm{sgn}\,(\hat{\mathbf{u}}_i\cdot\hat{\mathbf{n}})\hat{\mathbf{n}}+\frac{2\tilde{W}A}{c}(\hat{\mathbf{v}}_i\cdot\hat{\mathbf{n}})^2\,\mathrm{sgn}\,(\hat{\mathbf{v}}_i\cdot\hat{\mathbf{n}})\hat{\mathbf{n}} \quad (23)$$

where signum function sgn is commonly defined by

$$\mathrm{sgn}(x) = \begin{cases} 1 & \text{if } x > 0 \\ 0 & \text{if } x = 0 \\ -1 & \text{if } x < 0. \end{cases}$$

The sgn$(\cdot)$ term accounts for required sign change due to the direction of forces acting on the solar sail. Using Eq. (18), then the net radiation force may be expressed as

$$\begin{aligned}\mathbf{F}_{SRP} + \mathbf{F}_{ARP} =& \frac{\mathfrak{L}_1 A}{2\pi c r_1^2}(\hat{\mathbf{u}}_i\cdot\hat{\mathbf{n}})^2\,\mathrm{sgn}\,(\hat{\mathbf{u}}_i\cdot\hat{\mathbf{n}})\hat{\mathbf{n}} \\ &+ \frac{\mathfrak{L}_2(\phi; r_2, \rho, d_2)A}{2\pi c r_2^2}(\hat{\mathbf{v}}_i\cdot\hat{\mathbf{n}})^2\,\mathrm{sgn}\,(\hat{\mathbf{v}}_i\cdot\hat{\mathbf{n}})\hat{\mathbf{n}} \end{aligned} \quad (24)$$

In terms of explicit angles the following can be defined

$$\cos\alpha = \hat{\mathbf{u}}_i\cdot\hat{\mathbf{n}} \quad (25)$$

$$\cos(\psi-\alpha) = \hat{\mathbf{v}}_i\cdot\hat{\mathbf{n}} \quad (26)$$

Using the definition of sail loading $\sigma = m_3/A$ and $F_{SRP} + F_{ARP} = m_3\sum\mathbf{a}$, then

$$\sum\mathbf{a} = \frac{F_{SRP}+F_{ARP}}{\sigma A} \quad (27)$$

For a solar sail on orbit around m_1 the direction of incidence of radiation $\hat{\mathbf{u}}_i$ is defined by the unit vector $\hat{\mathbf{r}}_1$. Likewise for orbit around m_2, $\hat{\mathbf{v}}_i$ is defined as $\hat{\mathbf{r}}_2$. Thus Eq. (27) can be expressed as

$$\begin{aligned}\sum\mathbf{a} =& \frac{\mathfrak{L}_1}{2\pi c\sigma r_1^2}\cos^2\alpha\,\mathrm{sgn}\,(\hat{\mathbf{r}}_1\cdot\hat{\mathbf{n}})\hat{\mathbf{n}} \\ &+ \frac{\mathfrak{L}_2(\phi; r_2, \rho, d_2)}{2\pi c\sigma r_2^2}\cos^2(\psi-\alpha)\,\mathrm{sgn}\,(\hat{\mathbf{r}}_2\cdot\hat{\mathbf{n}})\hat{\mathbf{n}} \end{aligned} \quad (28)$$

In order to simplify for the nondimensional total acceleration of the solar sail due to SRP and ARP, then by using Eq. (4) and (5), Eq. (28) may be expressed as

$$\sum \mathbf{a} = \beta \frac{Gm_1}{r_1^2}(\hat{\mathbf{r}}_1 \cdot \hat{\mathbf{n}})^2 \operatorname{sgn}(\hat{\mathbf{r}}_1 \cdot \hat{\mathbf{n}})\hat{\mathbf{n}} + \tilde{\beta}\frac{Gm_2}{r_2^2}(\hat{\mathbf{r}}_2 \cdot \hat{\mathbf{n}})^2 \operatorname{sgn}(\hat{\mathbf{r}}_2 \cdot \hat{\mathbf{n}})\hat{\mathbf{n}} \tag{29}$$

where

$$\tilde{\beta} = \frac{\tilde{\sigma}^*}{\sigma} \tag{30}$$

and

$$\tilde{\sigma}^* = \frac{\mathfrak{L}_2(\phi; r_2, \rho, d_2)}{2\pi G m_2 c} \tag{31}$$

In a nondimensionalized CR3BP system, Eq. (29) may be expressed as

$$\sum \mathbf{a} = \beta \frac{(1-\mu)}{r_1^2}(\hat{\mathbf{r}}_1 \cdot \hat{\mathbf{n}})^2 \operatorname{sgn}(\hat{\mathbf{r}}_1 \cdot \hat{\mathbf{n}})\hat{\mathbf{n}} + \tilde{\beta}\frac{\mu}{r_2^2}(\hat{\mathbf{r}}_2 \cdot \hat{\mathbf{n}})^2 \operatorname{sgn}(\hat{\mathbf{r}}_2 \cdot \hat{\mathbf{n}})\hat{\mathbf{n}} \tag{32}$$

Looking at Eq. (30) and Eq. (31), then it is evident that the relationship between β and $\tilde{\beta}$ is of the form

$$\begin{aligned} \frac{\tilde{\beta}}{\beta} &= \frac{m_1}{m_2}\frac{\mathfrak{L}_2(\phi; r_2, \rho, d_2)}{\mathfrak{L}_1} \\ &= \frac{(1-\mu)}{\mu} D(\phi; r_2, \rho, d_2) \\ \Rightarrow \tilde{\beta} &= \beta \frac{(1-\mu)}{\mu} D(\phi; r_2, \rho, d_2) \end{aligned} \tag{33}$$

It can be inferred that $\tilde{\beta} = \beta$ when the function $D(\phi; r_2, \rho, d_2) = \mu/(1-\mu)$. This indicates the sail lightness numbers due to SRP and ARP are equal at a certain phase angle ϕ and distance r_2 for a given system with constant masses m_1 and m_2, albedo ρ and diameter d_2.
Eq. (32) may be explicitly decomposed into accelerations due to SRP and ARP, $\mathbf{a}_1$ and $\mathbf{a}_2$ respectively. The ARP acceleration, second term on the right hand side of Eq. (32), may then be expressed as

$$\mathbf{a}_2 = \tilde{\beta}\frac{\mu}{r_2^2}(\hat{\mathbf{r}}_2 \cdot \hat{\mathbf{n}})^2 \operatorname{sgn}(\hat{\mathbf{r}}_2 \cdot \hat{\mathbf{n}})\hat{\mathbf{n}} \tag{34}$$

The scalar form of solar sail EoM added with ARP are of the form

$$\ddot{x} - 2\dot{y} = -U_x + a_{1,x} + a_{2,x} \tag{35}$$

$$\ddot{y} + 2\dot{x} = -U_y + a_{1,y} + a_{2,y} \tag{36}$$

$$\ddot{z} = -U_z + a_{1,z} + a_{2,z} \tag{37}$$

At equilibrium solutions, Eq. (2) is modified to be

$$\dot{\mathbf{x}} = \begin{bmatrix} \dot{\mathbf{r}} \\ \ddot{\mathbf{r}} \end{bmatrix} = \mathbf{0}_{6\times 1} = \begin{bmatrix} \mathbf{0}_{3\times 1} \\ \mathbf{a}_1 + \mathbf{a}_2 - \boldsymbol{\nabla} U \end{bmatrix}_{6\times 1} \tag{38}$$

Taking the scalar product of Eq. (32) with $\hat{\mathbf{n}}$, and requiring equilibrium solutions then

$$(\mathbf{a}_1 + \mathbf{a}_2) \cdot \hat{\mathbf{n}} = \boldsymbol{\nabla} U \cdot \hat{\mathbf{n}} \tag{39}$$

$$\left(\beta \frac{(1-\mu)}{r_1^2} (\hat{\mathbf{r}}_1 \cdot \hat{\mathbf{n}})^2 \operatorname{sgn}(\hat{\mathbf{r}}_1 \cdot \hat{\mathbf{n}}) \hat{\mathbf{n}} + \tilde{\beta} \frac{\mu}{r_2^2} (\hat{\mathbf{r}}_2 \cdot \hat{\mathbf{n}})^2 \operatorname{sgn}(\hat{\mathbf{r}}_2 \cdot \hat{\mathbf{n}}) \hat{\mathbf{n}} \right) \cdot \hat{\mathbf{n}} = \boldsymbol{\nabla} U \cdot \hat{\mathbf{n}} \tag{40}$$

$$\beta \frac{(1-\mu)}{r_1^2} (\hat{\mathbf{r}}_1 \cdot \hat{\mathbf{n}})^2 \operatorname{sgn}(\hat{\mathbf{r}}_1 \cdot \hat{\mathbf{n}}) + \tilde{\beta} \frac{\mu}{r_2^2} (\hat{\mathbf{r}}_2 \cdot \hat{\mathbf{n}})^2 \operatorname{sgn}(\hat{\mathbf{r}}_2 \cdot \hat{\mathbf{n}}) = \boldsymbol{\nabla} U \cdot \hat{\mathbf{n}} \tag{41}$$

Substituting Eq. (34) into Eq. (41), then the following is obtained

$$\beta(1-\mu) \left(\frac{1}{r_1^2} (\hat{\mathbf{r}}_1 \cdot \hat{\mathbf{n}})^2 \operatorname{sgn}(\hat{\mathbf{r}}_1 \cdot \hat{\mathbf{n}}) + \frac{D(\phi; r_2, \rho, d_2)}{r_2^2} (\hat{\mathbf{r}}_2 \cdot \hat{\mathbf{n}})^2 \operatorname{sgn}(\hat{\mathbf{r}}_2 \cdot \hat{\mathbf{n}}) \right) = \boldsymbol{\nabla} U \cdot \hat{\mathbf{n}} \tag{42}$$

Since it is required that $\boldsymbol{\nabla} U \cdot \hat{\mathbf{n}} \geq 0$ or $(\mathbf{a}_1 + \mathbf{a}_2) \cdot \hat{\mathbf{n}} \geq 0$, then there exist four analytical forms due to the sgn operator of which only three are physically

valid and satisfy the condition $\sum \mathbf{a} \cdot \hat{\mathbf{n}} \geq 0$, i.e.

$$\sum \mathbf{a} \cdot \hat{\mathbf{n}} = \begin{cases} \beta(1-\mu)\left(\frac{1}{r_1^2}(\hat{\mathbf{r}}_1 \cdot \hat{\mathbf{n}})^2 + \frac{D(\phi; r_2, \rho, d_2)}{r_2^2}(\hat{\mathbf{r}}_2 \cdot \hat{\mathbf{n}})^2\right) & \text{if case 1;} \\ \beta(1-\mu)\left(\frac{1}{r_1^2}(\hat{\mathbf{r}}_1 \cdot \hat{\mathbf{n}})^2 - \frac{D(\phi; r_2, \rho, d_2)}{r_2^2}(\hat{\mathbf{r}}_2 \cdot \hat{\mathbf{n}})^2\right) & \text{if case 2;} \\ \beta(1-\mu)\left(-\frac{1}{r_1^2}(\hat{\mathbf{r}}_1 \cdot \hat{\mathbf{n}})^2 + \frac{D(\phi; r_2, \rho, d_2)}{r_2^2}(\hat{\mathbf{r}}_2 \cdot \hat{\mathbf{n}})^2\right) & \text{if case 3;} \\ \text{Undefined} & \text{if case 4.} \end{cases} \tag{43}$$

where case 1: $\hat{\mathbf{r}}_1 \cdot \hat{\mathbf{n}} \geq 0$, $\hat{\mathbf{r}}_2 \cdot \hat{\mathbf{n}} \geq 0$ and $\sum \mathbf{a} \cdot \hat{\mathbf{n}} \geq 0$; case 2: $\hat{\mathbf{r}}_1 \cdot \hat{\mathbf{n}} \geq 0$, $\hat{\mathbf{r}}_2 \cdot \hat{\mathbf{n}} < 0$ and $\sum \mathbf{a} \cdot \hat{\mathbf{n}} \geq 0$; case 3: $\hat{\mathbf{r}}_1 \cdot \hat{\mathbf{n}} < 0$, $\hat{\mathbf{r}}_2 \cdot \hat{\mathbf{n}} \geq 0$ and $\sum \mathbf{a} \cdot \hat{\mathbf{n}} \geq 0$ and case 4: $\hat{\mathbf{r}}_1 \cdot \hat{\mathbf{n}} < 0$, $\hat{\mathbf{r}}_2 \cdot \hat{\mathbf{n}} < 0$ and $\sum \mathbf{a} \cdot \hat{\mathbf{n}} < 0$. The solar sail may now have the normal vector $\hat{\mathbf{n}}$ directed against either bodies m_1 and m_2 but not both at the same time, i.e. $\hat{\mathbf{n}}$ may now be directed against SRP or ARP, contrary to previous work if only SRP is accounted for (McInnes et al., 1994). Rearranging Eq. (42) then the equilibrium solutions may be parametrized by β as

$$\beta = \frac{\boldsymbol{\nabla} U \cdot \hat{\mathbf{n}}}{(1-\mu)\langle \frac{1}{r_1^2}(\hat{\mathbf{r}}_1 \cdot \hat{\mathbf{n}})^2 \operatorname{sgn}(\hat{\mathbf{r}}_1 \cdot \hat{\mathbf{n}}) + \frac{D(\phi; r_2, \rho, d_2)}{r_2^2}(\hat{\mathbf{r}}_2 \cdot \hat{\mathbf{n}})^2 \operatorname{sgn}(\hat{\mathbf{r}}_2 \cdot \hat{\mathbf{n}})\rangle} \tag{44}$$

where the $\langle \cdot \rangle$ is now the nonnegative operator. Eq. (44) is referred to as contribution (a) in section 1 and serves as an extension to previous work (McInnes et al., 1994; McInnes, 1999). A value for β will be given at any specific equilibrium point. Equivalently equilibrium surfaces can be rendered for any chosen specific values of β. Eq. (43) is now also a function of phase angle, orientation and distance with respect to the second primary mass as well as the object diameter, which all characterize the ARP exerted on the solar sail. For simplicity in this paper and comparison to previous work (McInnes et al., 1994; McInnes, 1999), Eq. (44) is parametrized by β instead of $\tilde{\beta}$, as it is the intuitive design parameter to use as a benchmark since ARP is inherently a function of SRP. This choice also provides flexibility since the three body system may change in a mission scenario when surveying multiple objects. Furthermore, mass and area of the spacecraft may be selected based on the solar sail lightness number desired.

3.2. Constraints on the Existence of Equilibrium Solutions

Now in order to analyze a meaningful constraint for both SRP and ARP affecting the solar sail together, then at an equilibrium solutions it is required

that Eq. (1) will be in a motionless condition of the solar sail, i.e.

$$\boldsymbol{\nabla} U = \mathbf{a}_1 + \mathbf{a}_2 \tag{45}$$

Evaluating the gradient of the pseudo-potential U, defined in Appendix A, and taking the scalar product of Eq. (45) with $\hat{\mathbf{n}}$, it is required that $\beta \geq 0$ i.e. the solar sail lightness number is lower bounded and that $\boldsymbol{\nabla} U \cdot \hat{\mathbf{n}} \geq 0$ or $(\mathbf{a}_1 + \mathbf{a}_2) \cdot \hat{\mathbf{n}} \geq 0$. The following boundaries are therefore derived as

$$\begin{aligned} \boldsymbol{\nabla} U \cdot \hat{\mathbf{n}} &= 0 \\ \boldsymbol{\nabla} U \cdot \frac{\boldsymbol{\nabla} U}{\|\boldsymbol{\nabla} U\|_2} &= 0 \\ \|\boldsymbol{\nabla} U\|_2 &= 0 \end{aligned} \tag{46}$$

or alternatively two boundaries can be derived in terms of $\mathbf{a}_1 + \mathbf{a}_2$ which corresponds to the denominator in Eq. (45) i.e. when $\beta \to \infty$, then

$$\begin{aligned} (\mathbf{a}_1 + \mathbf{a}_2) \cdot \hat{\mathbf{n}} &= 0 \\ \beta \frac{(1-\mu)}{r_1^2} (\hat{\mathbf{r}}_1 \cdot \hat{\mathbf{n}})^2 \operatorname{sgn}(\hat{\mathbf{r}}_1 \cdot \hat{\mathbf{n}}) + \tilde{\beta} \frac{\mu}{r_2^2} (\hat{\mathbf{r}}_2 \cdot \hat{\mathbf{n}})^2 \operatorname{sgn}(\hat{\mathbf{r}}_1 \cdot \hat{\mathbf{n}}) &= 0 \\ \beta(1-\mu) \left(\frac{1}{r_1^2} (\hat{\mathbf{r}}_1 \cdot \hat{\mathbf{n}})^2 \operatorname{sgn}(\hat{\mathbf{r}}_1 \cdot \hat{\mathbf{n}}) + \frac{D(\phi; r_2, \rho, d_2)}{r_2^2} (\hat{\mathbf{r}}_2 \cdot \hat{\mathbf{n}})^2 \operatorname{sgn}(\hat{\mathbf{r}}_2 \cdot \hat{\mathbf{n}}) \right) &= 0 \\ \frac{1}{r_1^2} (\hat{\mathbf{r}}_1 \cdot \hat{\mathbf{n}})^2 \operatorname{sgn}(\hat{\mathbf{r}}_1 \cdot \hat{\mathbf{n}}) + \frac{D(\phi; r_2, \rho, d_2)}{r_2^2} (\hat{\mathbf{r}}_2 \cdot \hat{\mathbf{n}})^2 \operatorname{sgn}(\hat{\mathbf{r}}_2 \cdot \hat{\mathbf{n}}) &= 0 \\ r_2^2 (\hat{\mathbf{r}}_1 \cdot \hat{\mathbf{n}})^2 \operatorname{sgn}(\hat{\mathbf{r}}_1 \cdot \hat{\mathbf{n}}) + r_1^2 D(\phi; r_2, \rho, d_2) (\hat{\mathbf{r}}_2 \cdot \hat{\mathbf{n}})^2 \operatorname{sgn}(\hat{\mathbf{r}}_2 \cdot \hat{\mathbf{n}}) &= 0 \end{aligned}$$

The derived result defines a boundary as a function of albedo effects, for where equilibrium solutions exist and do not exist for $\beta \geq 0$ when both SRP and ARP are exerted on the solar sail. In the free areas the solar sail may now orient itself unreservedly and there are no constraints on $|\alpha|$ and $|(\psi - \alpha)|$ as long as the condition $(\mathbf{a}_1 + \mathbf{a}_2) \geq 0$ is satisfied. For case 1 and 4 the derived result will correspond to the function $V(\mathbf{r}_1, \mathbf{r}_2)$ and is defined as

$$V(\mathbf{r}_1, \mathbf{r}_2) = r_2^2 (\hat{\mathbf{r}}_1 \cdot \hat{\mathbf{n}})^2 + r_1^2 D(\phi; r_2, \rho, d_2) (\hat{\mathbf{r}}_2 \cdot \hat{\mathbf{n}})^2 = 0 \tag{47}$$

For case 2 and 3 the function $\tilde{V}(\mathbf{r}_1, \mathbf{r}_2) = 0$ may be defined as

$$\tilde{V}(\mathbf{r}_1, \mathbf{r}_2) = r_2^2 (\hat{\mathbf{r}}_1 \cdot \hat{\mathbf{n}})^2 - r_1^2 D(\phi; r_2, \rho, d_2) (\hat{\mathbf{r}}_2 \cdot \hat{\mathbf{n}})^2 = 0 \tag{48}$$

$V(\mathbf{r}_1, \mathbf{r}_2)$ corresponds to when $\hat{\mathbf{n}}$ is pointed away from (case 1) or against (case 4) both SRP and ARP at the same time. The latter case is not practically valid since the solar sail may not accelerate towards both m_1 and m_2 simultaneously. This boundary shows where the equilibrium solutions may not exist when the sail experiences forces on the same side. Similar to $S(\mathbf{r}_1, \mathbf{r}_2)$, the boundary exists in form of two topologically disconnected surfaces. Boundary $\tilde{V}(\mathbf{r}_1, \mathbf{r}_2)$ shows where the equilibrium solutions may not exist when the sail experiences forces on its opposites. $\tilde{V}(\mathbf{r}_1, \mathbf{r}_2)$ corresponds to when $\hat{\mathbf{n}}$ is pointed against SRP and away from ARP, defined as case 2, or against ARP and away from SRP, defined as case 3. The result is referred to contribution (b) in section 1 and practically this means that the solar sail may orient itself to $0° < |\alpha| < 180°$ and still retain equilibrium solutions at a chosen attitude. Equivalently it can orient itself to $|\alpha| \geq 90°$ in some of the areas previously known to be forbidden in the model with SRP alone, defined by the boundary $S(\mathbf{r}_1, \mathbf{r}_2)$ in Eq. (11) (McInnes, 1999). It can be inferred that if $D(\phi; r_2, \rho, d_2) = 0$ or $\rho = 0$, i.e. when there are no albedo effects, then Eq. (47) and Eq. (48) reduce to the constraint $V(\mathbf{r}_1, \mathbf{r}_2) = S(\mathbf{r}_1, \mathbf{r}_2)$ as presented in McInnes (1999).

3.3. Photometric Regions of Influence

Since there are now two acceleration forces to balance the gravitational force to achieve equilibrium, it is important to establish the scale of influence of SRP and ARP to see which force affects the solar sail the most in vicinity of m_2. Here the derivation of the magnitude of the SRP and ARP accelerations $\|\mathbf{a}_1\|_2$ and $\|\mathbf{a}_2\|_2$ are given and analyzed when they are equal thus defining the boundary, similar to the mathematical definition for sphere of influence (SoI) as presented in Battin (1999). A region of influence (RoI) created by the luminosity of m_2 exists between the boundary $\|\mathbf{a}_1\|_2 - \|\mathbf{a}_2\|_2 = 0$ and the object m_2 and is derived as follows

$$\|\mathbf{a}_1\|_2 = \|\mathbf{a}_2\|_2 \tag{49}$$

$$\left\|\beta\frac{(1-\mu)}{r_1^2}(\hat{\mathbf{r}}_1\cdot\hat{\mathbf{n}})^2\,\mathrm{sgn}\,(\hat{\mathbf{r}}_1\cdot\hat{\mathbf{n}})\right\|_2 = \left\|\tilde{\beta}\frac{\mu}{r_2^2}(\hat{\mathbf{r}}_2\cdot\hat{\mathbf{n}})^2\,\mathrm{sgn}\,(\hat{\mathbf{r}}_2\cdot\hat{\mathbf{n}})\right\|_2$$

$$\Rightarrow \left\|\beta\frac{(1-\mu)}{r_1^2}(\hat{\mathbf{r}}_1\cdot\hat{\mathbf{n}})^2\right\|_2 = \left\|\beta\frac{\mu(1-\mu)D(\phi;r_2,\rho,d_2)}{\mu r_2^2}(\hat{\mathbf{r}}_2\cdot\hat{\mathbf{n}})^2\right\|_2$$

$$\Rightarrow \left\|\frac{1}{r_1^2}(\hat{\mathbf{r}}_1\cdot\hat{\mathbf{n}})^2\right\|_2 = \left\|\frac{D(\phi;r_2,\rho,d_2)}{r_2^2}(\hat{\mathbf{r}}_2\cdot\hat{\mathbf{n}})^2\right\|_2 \tag{50}$$

$$\|\mathbf{a}_1\|_2 - \|\mathbf{a}_2\|_2 = \left\|\frac{1}{r_1^2}(\hat{\mathbf{r}}_1\cdot\hat{\mathbf{n}})^2\right\|_2 - \left\|\frac{D(\phi;r_2,\rho,d_2)}{r_2^2}(\hat{\mathbf{r}}_2\cdot\hat{\mathbf{n}})^2\right\|_2 = 0 \tag{51}$$

or simplified as

$$\left(\frac{r_2}{r_1}\right)^2 = D(\phi;r_2,\rho,d_2)\frac{(\hat{\mathbf{r}}_2\cdot\hat{\mathbf{n}})^2}{(\hat{\mathbf{r}}_1\cdot\hat{\mathbf{n}})^2} \tag{52}$$

or

$$r_{RoI} \equiv r_2 = r_1 D(\phi;r_2,\rho,d_2)^{1/2}\frac{\cos(\psi-\alpha)}{\cos\alpha} \tag{53}$$

where $r_{RoI} = r_2$ and is the distance from m_2 to the RoI boundary $\|\mathbf{a}_1\|_2 - \|\mathbf{a}_2\|_2 = 0$. This boundary indicates where the SRP acceleration is larger than ARP acceleration i.e. where $\|\mathbf{a}_1\|_2 > \|\mathbf{a}_2\|_2$ and vice versa. The result is referred to as contribution (c) in section 1. For close-up observations of m_2, at a distance of $r_2 < 1,000\,m$ for an instance, this particular contribution is important to emphasize since its impact on the solar sail dynamics has been analytically identified for which Eq. (43) is a fundamental cause thereof. In such a condition the solar sail would be strongly influenced by ARP and therefore equilibrium solutions in the RoI would alter significantly as $\|\mathbf{a}_1\|_2 < \|\mathbf{a}_2\|_2$. Moreover $\|\mathbf{a}_1\|_2 << \|\mathbf{a}_2\|_2$ when the solar sail is very close to the object m_2. On the other hand, when $\|\mathbf{a}_1\|_2 > \|\mathbf{a}_2\|_2$ equilibrium solutions would not be significantly altered.

Now that the solar sail dynamics in CR3BP with SRP have been properly defined, it is worth looking into the stability of the artificial equilibrium points and how to locally control the spacecraft if the equilibrium points are naturally unstable.

4. Stability and Control at Libration Points

In reality, the motion of a spacecraft in CR3BP is highly nonlinear and complex. In order to investigate stability and controllability, the behavior of the system is analyzed using local linear dynamics about the chosen equilib-

rium points of interest, e.g. the Lagrangian points or artificial equilibrium points. This section intentionally presents the methodology and notation very similar to McInnes et al. (1994); McInnes (1999) in order to better understand the similarities and differences to previous studies.

The equilibrium (libration) points have the coordinates $(x_{L_i}, y_{L_i}, z_{L_i})$ in the rotating reference frame and L_i is the equilibrium point of interest. With perturbation at an equilibrium point the coordinates $(\delta x, \delta y, \delta z)$ may be written as

$$\mathbf{r}_{L_i} + \delta\mathbf{r} = \left[(x_{Li} + \delta x)\ (y_{Li} + \delta y)\ (z_{Li} + \delta z)\right]^T \tag{54}$$

With only first order terms considered from the Taylor Series Expansion, the local solar sail EoM with respect to the equilibrium points at $\mathbf{r}_{L_i}$ (denoted with $'^*'$) are expressed as

$$\begin{aligned}
\delta\ddot{x} - 2\delta\dot{y} =& (-U^*_{xx} + a^*_{1,xx} + a^*_{2,xx})\delta x + (-U^*_{xy} + a^*_{1,xy} + a^*_{2,xy})\delta y \\
&+ (-U^*_{xz} + a^*_{1,xz} + a^*_{2,xz})\delta z \qquad (55)\\
\delta\ddot{y} + 2\delta\dot{x} =& (-U^*_{yx} + a^*_{1,yx} + a^*_{2,yx})\delta x + (-U^*_{yy} + a^*_{1,yy} + a^*_{2,yy})\delta y \\
&+ (-U^*_{yz} + a^*_{1,yz} + a^*_{2,yz})\delta z \qquad (56)\\
\delta\ddot{z} =& (-U^*_{zx} + a^*_{1,zx} + a^*_{2,zx})\delta x + (-U^*_{zy} + a^*_{1,zy} + a^*_{2,zy})\delta y \\
&+ (-U^*_{zz} + a^*_{1,zz} + a^*_{2,zz})\delta z \qquad (57)
\end{aligned}$$

where $U_{jk} = \partial U/\partial j\partial k$ and $U^*_{jk} = U_{jk}|_{L_i}$ where $(j,k) \in (x,y,z)$. These partials are given in Appendix B. The second partials of the acceleration terms $\mathbf{a}_1$ and $\mathbf{a}_2$ are defined as $a_{j,kl} = \partial a_j/\partial k\partial l$ and is the lth derivative of the kth component of the radiation acceleration vector $\mathbf{a}_j$ with respect to body m_j $j \in (1,2)$, and furthermore $a^*_{j,kl} = a_{j,kl}|_{L_i}$. The first and second partials of the accelerations are given in Appendix C and Appendix D respectively.

In state space form the perturbation dynamics may be written as

$$\dot{\tilde{\mathbf{x}}} = \mathbf{A}\tilde{\mathbf{x}} \tag{58}$$

where the state vector is defined as $\tilde{\mathbf{x}} = [\delta x\ \delta y\ \delta z\ \delta\dot{x}\ \delta\dot{y}\ \delta\dot{z}]^T$ and the state matrix $\mathbf{A} \in \mathbb{R}^{6\times 6}$ is defined as

$$\mathbf{A} = \begin{bmatrix} \mathbf{0}_{3\times 3} & \mathbb{I}_{3\times 3} \\ \mathbf{T} & \mathbf{N} \end{bmatrix} \tag{59}$$

where

$$\mathbf{T} = \begin{bmatrix} -U_{xx} + a_{1,xx} + a_{2,xx} & -U_{xy} + a_{1,xy} + a_{2,xy} & -U_{xz} + a_{1,xz} + a_{2,xz} \\ -U_{yx} + a_{1,yx} + a_{2,yx} & -U_{yy} + a_{1,yy} + a_{2,yy} & -U_{yz} + a_{1,yz} + a_{2,yz} \\ -U_{zx} + a_{1,zx} + a_{2,zx} & -U_{zy} + a_{1,zy} + a_{2,zy} & -U_{zz} + a_{1,zz} + a_{2,zz} \end{bmatrix} \tag{60}$$

$$\mathbf{N} = \begin{bmatrix} 0 & 2 & 0 \\ -2 & 0 & 0 \\ 0 & 0 & 0 \end{bmatrix} \tag{61}$$

For a nontrivial solution, then taking $\det(\mathbf{A}) = 0$ gives the characteristic polynomial (McInnes et al., 1994)

$$\mathfrak{P}(\lambda) = \sum_{j=0}^{6} q_j \lambda^{6-j} \tag{62}$$

It is known that in the system without SRP the collinear libration points, L_1, L_2, L_3, are unstable and the initial conditions can at best be chosen such that the eigenvalues are not excited, meaning Lyapunov stability may be achieved close to the collinear points (Nuss, 1998).
The coefficients of the polynomial $\mathfrak{P}(\lambda)$ are given by (McInnes et al., 1994)

$$\begin{aligned} q_6 &= \mathbf{T}^*_{11}(\mathbf{T}^*_{22}\mathbf{T}^*_{33} - \mathbf{T}^*_{23}\mathbf{T}^*_{32}) - \mathbf{T}^*_{12}(\mathbf{T}^*_{33}\mathbf{T}^*_{21} - \mathbf{T}^*_{23}\mathbf{T}^*_{31}) \\ &\quad - \mathbf{T}^*_{13}(\mathbf{T}^*_{22}\mathbf{T}^*_{31} - \mathbf{T}^*_{21}\mathbf{T}^*_{32}) && \text{(63a)} \\ q_5 &= 2\mathbf{T}^*_{33}(\mathbf{T}^*_{21}\mathbf{T}^*_{12}) + 2(\mathbf{T}^*_{32}\mathbf{T}^*_{13} - \mathbf{T}^*_{23}\mathbf{T}^*_{31}) && \text{(63b)} \\ q_4 &= \mathbf{T}^*_{11}\mathbf{T}^*_{22} + \mathbf{T}^*_{11}\mathbf{T}^*_{33} + \mathbf{T}^*_{23}\mathbf{T}^*_{32} - \mathbf{T}^*_{13}\mathbf{T}^*_{31} - \mathbf{T}^*_{12}\mathbf{T}^*_{21} + 4\mathbf{T}^*_{33} && \text{(63c)} \\ q_3 &= 2(\mathbf{T}^*_{21} - \mathbf{T}^*_{12}) && \text{(63d)} \\ q_2 &= \mathbf{T}^*_{11} + \mathbf{T}^*_{22} + \mathbf{T}^*_{33} + 4 && \text{(63e)} \\ q_1 &= 0 && \text{(63f)} \\ q_0 &= 1 && \text{(63g)} \end{aligned}$$

To check if the system is stable then according to the Routh-Hurwitz criterion, then for a nth-degree polynomial $\mathfrak{P}(\lambda)$, all coefficients q_i must exist ($q_i \neq 0$), be positive $q_i > 0$ and if there is any sign change in the Routh Array then it means that the system is unstable. Looking at the Eqs. (63a)-(63g) implies that at least one eigenvalue will not lie in closed left half-plane (CLHP) of the root locus diagram since $q_1 = 0$. Thus the system is naturally unstable. Substituting for purely imaginary eigenvalues $\lambda = \iota\kappa$ ($\iota = \sqrt{-1}$),

the characteristic polynomial becomes as shown in (McInnes et al., 1994)

$$\mathfrak{P}(\iota\kappa) = -\kappa^6 + q_2\kappa^4 - \iota q_3\kappa^3 - q_4\kappa^2 + \iota q_5\kappa + q_6 \tag{64}$$

For the condition $\mathfrak{P}(\lambda) = 0$ then both real and purely imaginary parts are identically zero, thus

$$\kappa^6 + q_2\kappa^4 - q_4\kappa^2 + q_6 = 0 \tag{65a}$$

$$\iota\kappa(q_5 - \kappa^2 q_3) = 0 \tag{65b}$$

Six solutions appear from this set of equations with $\kappa_i^2 > 0$, $i = (1, ..., 6)$. With $\kappa_1 = 0$ and $\kappa_{2,3} = \pm\sqrt{\frac{q_5}{q_3}}$, the solution κ is not a consistent solution. The latter equation can be satisfied if $q_3 = q_5 = 0$ and are then represented in conjugate pairs in the first equation which may or may not have real solutions. In order to have Lyapunov stability then, by necessity, $q_3 = 0 \Rightarrow (\mathbf{T}_{21}^* - \mathbf{T}_{12}^*) = 0$. Since potential is conservative $U_{xy} - U_{yx} = 0$, such that $q_3 = 0 \Rightarrow (a_{1,yx} + a_{2,yx} - a_{1,xy} - a_{2,xy}) = 0$. With $q_5 = 0$ it is also required that $(a_{1,zx} + a_{2,zx} - a_{1,xz} - a_{2,xz}) = 0$ and $(a_{1,yz} + a_{2,yz} - a_{1,zy} - a_{2,zy}) = 0$. This implies that $\beta = 0$ or

$$\boldsymbol{\nabla} \times \mathbf{a}_1 + \boldsymbol{\nabla} \times \mathbf{a}_2 = \mathbf{0} \tag{66}$$

$$\Rightarrow \boldsymbol{\nabla} \times \mathbf{a}_1 = -\boldsymbol{\nabla} \times \mathbf{a}_2 \tag{67}$$

Similar to the CR3BP with SRP acceleration $\mathbf{a}_1$ only, this implies both $\mathbf{a}_1$ and $\mathbf{a}_2$ must be either conservative or one of the accelerations must be balanced by opposite curl. A requirement for Lyapunov stability is therefore that SRP force is zero, i.e. $\beta = 0$, or the problem is conservative, i.e. $|\alpha| = 90°$ and $\psi = 0°$ or $|\psi| = 180°$, or the accelerations are balanced, i.e. $\mathbf{a}_1 = -\mathbf{a}_2$. Interestingly enough, the condition $\mathbf{a}_1 = -\mathbf{a}_2$ occurs at the RoI boundary $V(\mathbf{r}_1, \mathbf{r}_2)$ as derived in Eq. (47). The modified stability characteristics are part of contribution (d) in section 1. Although the equilibrium solutions are in general unstable, they are controllable using either feedback to the sail attitude or trim to the sail area.

In this paper the sail controllability of position and velocity will be investigated using the solar sail attitude as the control input, which is considered to be more practical than trimming area of the solar sail by varying β as there is more flexibility in changing the attitude by two control variables

only. Nevertheless, in future work, it is worth to examine controllability with all three control variables as the thrust of the solar sail inherently has three components (McInnes, 2000). The sail orientation control variables are defined such that the input is

$$\mathbf{u}^* + \delta\mathbf{u} = [(\alpha_{L_i} + \delta\alpha) \ (\gamma_{L_i} + \delta\gamma)]^T \tag{68}$$

where α_{L_i} and γ_{L_i} are the nominal sail angles corresponding to the libration point of interest. Thus the state space form becomes

$$\dot{\tilde{\mathbf{x}}} = \mathbf{A}\tilde{\mathbf{x}} + \mathbf{B}\delta\mathbf{u} \tag{69}$$

where $\mathbf{A}$ is the same as defined in Eq. (59) and the input matrix $\mathbf{B} \in \mathbb{R}^{6\times 2}$ will now have the form

$$\mathbf{B} = \begin{bmatrix} \mathbf{0}_{3\times 2} \\ \tilde{\mathbf{a}}^* \end{bmatrix} \tag{70}$$

where

$$\tilde{\mathbf{a}}^* = \begin{bmatrix} a^*_{1,x\alpha} + a^*_{2,x\alpha} & a^*_{1,x\gamma} + a^*_{2,x\gamma} \\ a^*_{1,y\alpha} + a^*_{2,y\alpha} & a^*_{1,y\gamma} + a^*_{2,y\gamma} \\ a^*_{1,z\alpha} + a^*_{2,z\alpha} & a^*_{1,z\gamma} + a^*_{2,z\gamma} \end{bmatrix} \tag{71}$$

where $a_{j,kl} = \partial a_j / \partial k \partial l$ and is the lth derivative of the kth component of the radiation acceleration vector $\mathbf{a}_j$ with respect to body m_j, $j \in (1, 2)$, and furthermore $a^*_{j,kl} = a_{j,kl}|_{L_i}$. The partial derivatives are given in Appendix E and Appendix F.

The controllability matrix $\mathbf{\Gamma} \in \mathbb{R}^{6\times 12}$ may be written as

$$\mathbf{\Gamma} = \begin{bmatrix} \mathbf{B} & \mathbf{AB} & \mathbf{A}^2\mathbf{B} & \mathbf{A}^3\mathbf{B} & \mathbf{A}^4\mathbf{B} & \mathbf{A}^5\mathbf{B} \end{bmatrix} \tag{72}$$

To check for controllability, and noting that

$$\mathbf{N}^2 = \begin{bmatrix} -4 & 0 & 0 \\ 0 & -4 & 0 \\ 0 & 0 & 0 \end{bmatrix} \tag{73}$$

and $\mathbf{N}^3 = -4\mathbf{N}$, the $\mathbf{A}$ matrix and higher-order powers are the following

$$\mathbf{A}^2 = \begin{bmatrix} \mathbf{T} & \mathbf{N} \\ \mathbf{NT} & \mathbf{T} + \mathbf{N} \end{bmatrix} \tag{74}$$

$$\mathbf{A}^3 = \begin{bmatrix} \mathbf{NT} & \mathbf{N}^2 + \mathbf{T} \\ \mathbf{T}^2\mathbf{N}^2 + \mathbf{T}^2 & 2\mathbf{NT} - 4\mathbf{N} \end{bmatrix} \tag{75}$$

$$\mathbf{A}^4 = \begin{bmatrix} \mathbf{T}^2\mathbf{N}^2 + \mathbf{T}^2 & 2\mathbf{NT} - 4\mathbf{N} \\ -4\mathbf{TN} - 2\mathbf{TNT} & \mathbf{T}^2 - 4\mathbf{N}^2 - \mathbf{N}^2\mathbf{T} \end{bmatrix} \tag{76}$$

$$\mathbf{A}^5 = \begin{bmatrix} -4\mathbf{TN} - 2\mathbf{TNT} & \mathbf{T}^2 - 4\mathbf{N}^2 - \mathbf{N}^2\mathbf{T} \\ \mathbf{T}^3 - \mathbf{TN}^2\mathbf{T} - 4\mathbf{TN}^2 & 16\mathbf{N} - \mathbf{NT}^2 \end{bmatrix} \tag{77}$$

The controllability matrix may thus be expressed in terms of columns as

$$\mathbf{\Gamma} = \begin{bmatrix} \mathbf{w}_1 & \mathbf{w}_2 & \mathbf{w}_3 & \mathbf{w}_4 & \mathbf{w}_5 & \mathbf{w}_6 \end{bmatrix} \tag{78}$$

where,

$$\mathbf{w}_1 = \begin{bmatrix} \mathbf{0} \\ \tilde{\mathbf{a}}^* \end{bmatrix}; \tag{79}$$

$$\mathbf{w}_2 = \begin{bmatrix} \tilde{\mathbf{a}}^* \\ \mathbf{N}\tilde{\mathbf{a}}^* \end{bmatrix}; \tag{80}$$

$$\mathbf{w}_3 = \begin{bmatrix} \mathbf{N}\tilde{\mathbf{a}}^* \\ (\mathbf{T} + \mathbf{N})\tilde{\mathbf{a}}^* \end{bmatrix}; \tag{81}$$

$$\mathbf{w}_4 = \begin{bmatrix} (\mathbf{N}^2 + \mathbf{T})\tilde{\mathbf{a}}^* \\ (2\mathbf{NT} - 4\mathbf{N})\tilde{\mathbf{a}}^* \end{bmatrix}; \tag{82}$$

$$\mathbf{w}_5 = \begin{bmatrix} (2\mathbf{NT} - 4\mathbf{N})\tilde{\mathbf{a}}^* \\ (\mathbf{T}^2 - 4\mathbf{N}^2 - \mathbf{N}^2\mathbf{T})\tilde{\mathbf{a}}^* \end{bmatrix}; \tag{83}$$

$$\mathbf{w}_6 = \begin{bmatrix} (\mathbf{T}^2 - 4\mathbf{N}^2 - \mathbf{N}^2\mathbf{T})\tilde{\mathbf{a}}^* \\ (16\mathbf{N} - \mathbf{NT}^2)\tilde{\mathbf{a}}^* \end{bmatrix} \tag{84}$$

It is found that the controllability matrix $\mathbf{\Gamma}$ has full rank except when the solar sail is not oriented parallell to the SRP and ARP forces having the properties $\hat{\mathbf{r}}_1 \cdot \hat{\mathbf{n}} = 0$ and $\hat{\mathbf{r}}_2 \cdot \hat{\mathbf{n}} = 0$ simultaneously, i.e. when $|\alpha| = 90°$ and $|\psi| = 180°$ or $|\psi| = 0°$. This is naturally similar to the CR3BP with SRP acceleration $\mathbf{a}_1$ alone, i.e. when the system is uncontrollable if $\hat{\mathbf{r}}_1 \cdot \hat{\mathbf{n}} = 0$ as shown in McInnes et al. (1994). For $|\alpha| = 90°$ and $|\psi| = 180°$ and $|\psi| = 0°$, then the solar sail is positioned at the Lagrange points and no SRP and ARP effects are induced on the solar sail.
To prove the fact, let $\hat{\mathbf{r}}_1 \cdot \hat{\mathbf{n}} = 0$ and $\hat{\mathbf{r}}_2 \cdot \hat{\mathbf{n}} = 0$, then

$$\tilde{\mathbf{a}}^* = \begin{bmatrix} \mathbf{0}_{3\times3} \end{bmatrix} \tag{85}$$

and

$$\mathbf{B} = \mathbf{0}_{6\times 2} \tag{86}$$

The controllability matrix Γ becomes

$$\mathbf{\Gamma} = [\mathbf{0}_{6\times 2}\ \mathbf{0}_{6\times 2}\ \mathbf{0}_{6\times 2}\ \mathbf{0}_{6\times 2}\ \mathbf{0}_{6\times 2}\ \mathbf{0}_{6\times 2}] \tag{87}$$

Another case that may also render the system to be uncontrollable is when $a_{1,kl} = -a_{2,kl}$, and the following proves the fact

$$\tilde{\mathbf{a}}^* = \left[\mathbf{0}_{3\times 3}\right] \tag{88}$$

and

$$\mathbf{B} = \mathbf{0}_{6\times 2} \tag{89}$$

which gives the same result as Eq. (87).
Thus controllability depends mainly on $\mathbf{B}$ or $\tilde{\mathbf{a}}^*$. Hence columns $\mathbf{w}_{1-6}$ are all linearly dependent and system is uncontrollable. The findings presented in this section are referred to contribution (d) in this paper stated in section 1. This implies that the columns of $\mathbf{\Gamma}$ are linearly independent if and only if the first case $\hat{\mathbf{r}}_1 \cdot \hat{\mathbf{n}} \neq 0$ and $\hat{\mathbf{r}}_2 \cdot \hat{\mathbf{n}} \neq 0$ and second case $a_{1,kl} \neq -a_{2,kl}$, thus $\text{rank}(\mathbf{\Gamma}) = 6$ and the system is in general completely controllable.
Since the system generally is controllable, then a feedback gain $\mathbf{K}$ may be constructed by pole placement or optimal control such that the closed-loop system $\mathbf{A}_{cl} = (\mathbf{A} + \mathbf{BK})$ is asymptotically stable.

With the analytical framework established and derivations being shown as necessary for dynamics, stability and controllability, it is worthwile to look at the results retrieved through numerical simulation.

5. Numerical Results

This section will cover the simulation results achieved based on the theory established in sections 2 and 3. Analyzing the planar CR3BP for two separate cases: $y = 0$ and $z = 0$ the solar sail in the Sun-asteroid system with varying β and orientations (α, γ), it is clear that the classical libration points $L_{1,\ldots,5}$ are replaced by infinitely many artificial equilibrium points when including radiation pressure from both the Sun and the asteroid. For the results discussed here, the mass ratio μ, albedo ρ, diameter of asteroid d_2 and distance between Sun and the asteroid r_{12} are chosen to be as indicated in Table 2. These are geometrical and physical parameters equivalent to an

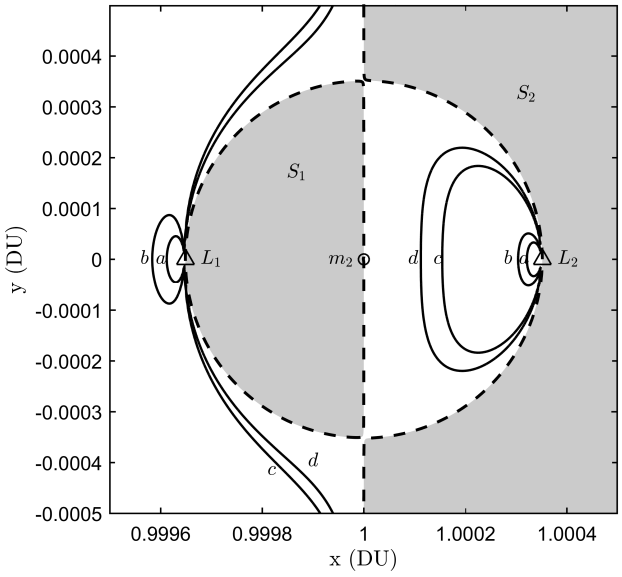

(a) $\hat{\mathbf{x}} - \hat{\mathbf{y}}$ Plane

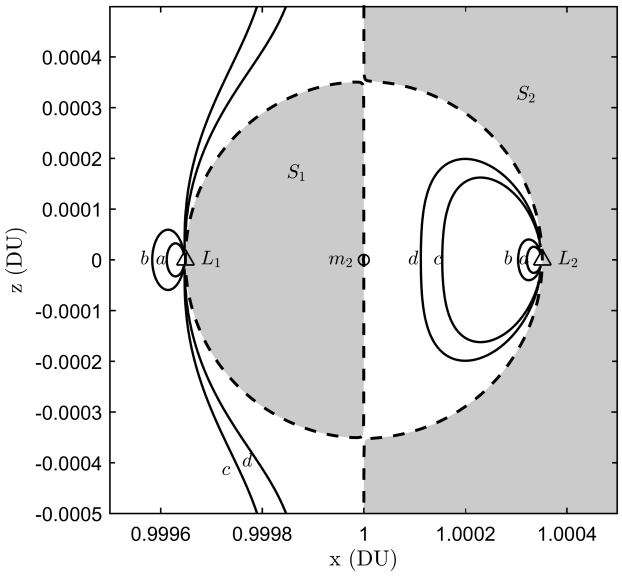

(b) $\hat{\mathbf{x}} - \hat{\mathbf{z}}$ Plane

Figure 3: Plots of equilibrium solutions by solar sail lightness number where ——— are the β contours, - - - is the boundary $S(\mathbf{r}_1, \mathbf{r}_2)$, $\triangle$ are the Lagrange points and $\circ$ is the asteroid

Table 2: CR3BP example parameters for Vesta

μ	ρ	$d_2\ (km)$	$r_{12}\ (km)$
1.3×10^{-10}	0.2	525.4	353.3×10^6

asteroid representing Vesta, which is a large asteroid residing in the asteroid field. Previous studies shown how SRP generates artificial equilibrium points (McInnes, 1999), however, with ARP these equilibrium points change considerably and solar lightness number surfaces at equilibra become altered due to the Lambertian BRDF as a function of ρ, d_2, ϕ and r_2. The chosen region to investigate is in the vicinity of L_1 and L_2.

Figs. 3a and 3b show some of the equilibrium solutions or contours of solar sail lightness number β in the CR3BP with SRP only in the $\hat{\mathbf{x}} - \hat{\mathbf{y}}$ plane and $\hat{\mathbf{x}} - \hat{\mathbf{z}}$ plane, respectively. Highlighted contours are $a : \beta = 0.0003$, $b : \beta = 0.0005$, $c : \beta = 0.005$, $d : \beta = 0.01$, similarly reproduced as in other literature (McInnes et al., 1994; McInnes, 1999, 2000; Nuss, 1998). The dashed lines indicate boundaries $S(\mathbf{r}_1, \mathbf{r}_2)$ which define the shaded areas where the β contours cannot exist as $\mathbf{r}_1 \cdot \hat{\mathbf{n}} \geq 0$ and be tangent to the mass m_2 and the collinear points L_1 and L_2. When $\boldsymbol{\nabla} U = \mathbf{0}$ or $\alpha = 90^\circ$ then the classical Lagrange points are retrieved.

Since μ is very small then this renders more flexibility for small numbers of β than for large β, demonstrated to be on the order of magnitude 10 less than for the Sun-Earth system (McInnes et al., 1994). This practically means that the solar radiation pressure force is much smaller than the solar gravitational force. For a balance between the solar radiation pressure force and the solar gravitational force the area to mass ratio is smaller thus a smaller solar sail area is required for a specific fixed mass. When $0.03 \leq \beta \leq 1$, the contours do not change considerably and thus flexibility is restricted to a smaller volume. If $0 \leq \beta \leq 1$ then the contour shows a three-dimensional nested torus projected onto the $\hat{\mathbf{x}} - \hat{\mathbf{y}}$ or $\hat{\mathbf{x}} - \hat{\mathbf{z}}$ plane. However for $\beta > 1$, then the inner radius of the torus disappears. As $\beta \to \infty$ the equilibrium surfaces approach the boundary $S(\mathbf{r}_1, \mathbf{r}_2)$. The equilibrium points have been demonstrated to be unstable but controllable in general (McInnes et al., 1994).

Figs. 4a and 4b show the three-dimensional surface of equilibrium solutions for $\beta = 0.0003$ and $\beta = 0.005$ and for $\beta = 0.0005$ and $\beta = 0.01$. Fig. 4b and Fig. 5b show the planar equilibrium solutions or contours of solar sail lightness number β in the CR3BP with both SRP and ARP in the

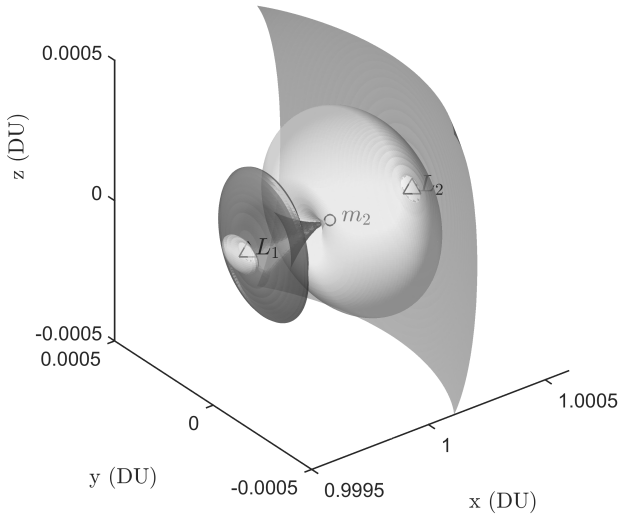

(a) $\beta = 0.0003$ (light) and $\beta = 0.005$ (dark)

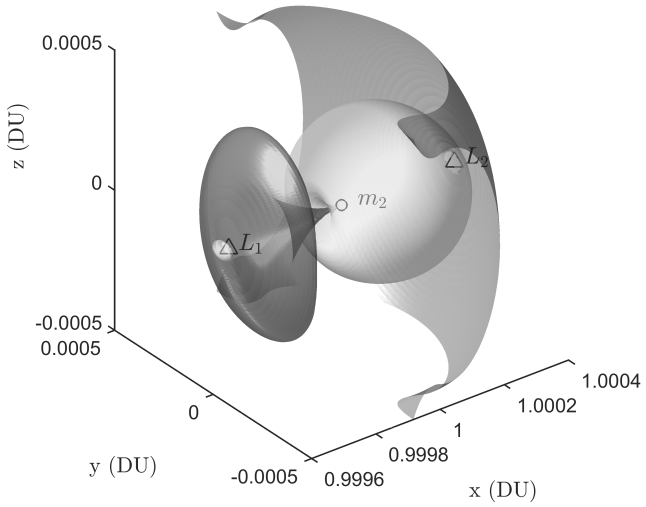

(b) $\beta = 0.0005$ (light) and $\beta = 0.01$ (dark)

Figure 4: Equilibrium surfaces with selected solar sail lightness numbers β where $\triangle$ are the Lagrange points and $\circ$ is the asteroid

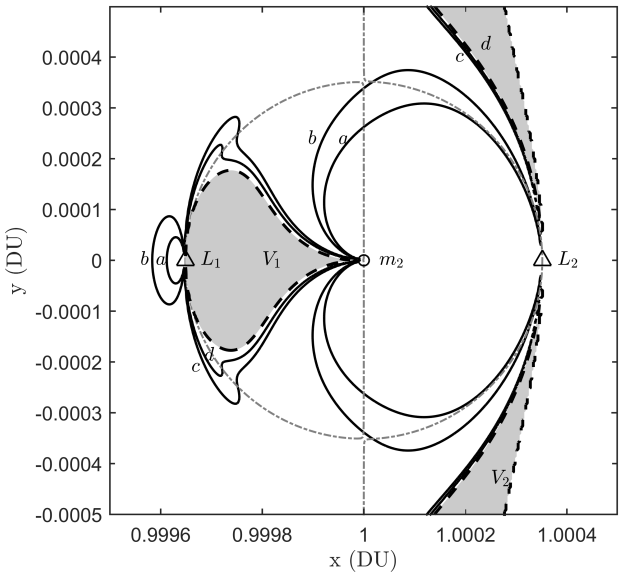

(a) $\hat{\mathbf{x}} - \hat{\mathbf{y}}$ Plane

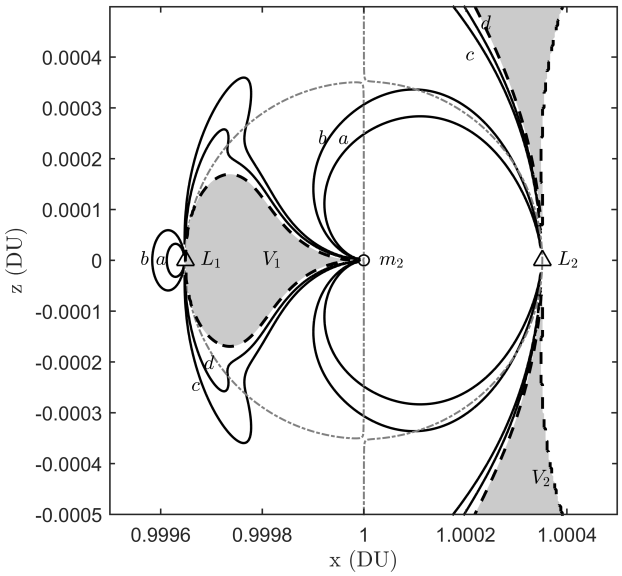

(b) $\hat{\mathbf{x}} - \hat{\mathbf{z}}$ Plane

Figure 5: Plots of equilibrium solutions by solar sail lightness number where ——— are the β contours, - - - is the boundary $V(\mathbf{r}_1, \mathbf{r}_2)$, - - - is the boundary $S(\mathbf{r}_1, \mathbf{r}_2)$, $\triangle$ are the Lagrange points and $\circ$ is the asteroid

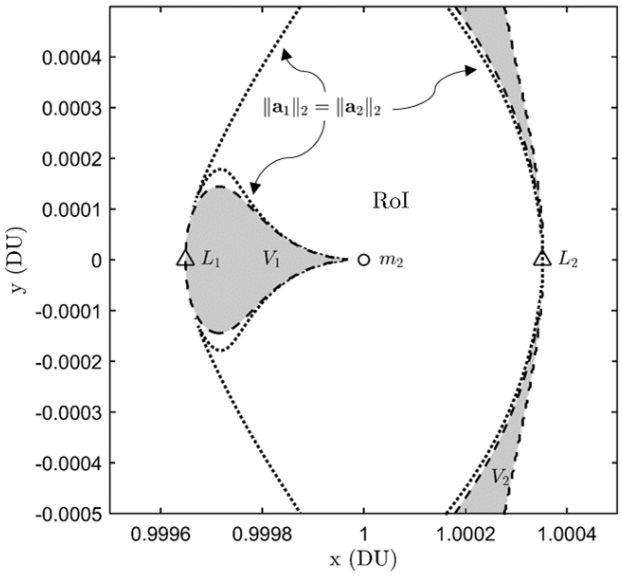

(a) $\hat{\mathbf{x}} - \hat{\mathbf{y}}$ Plane

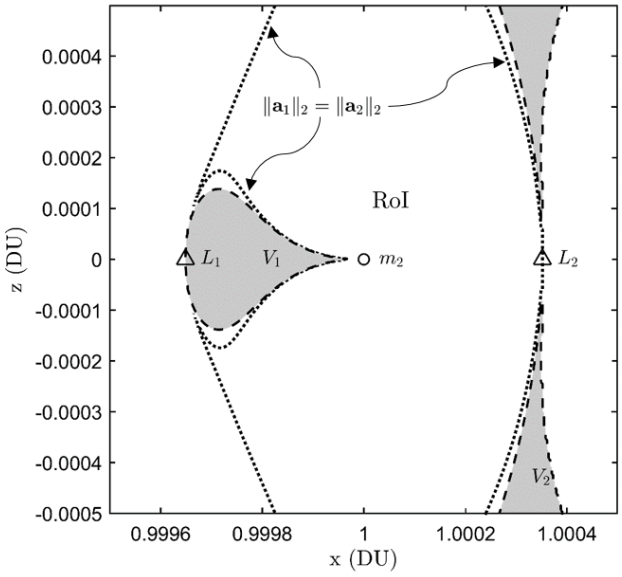

(b) $\hat{\mathbf{x}} - \hat{\mathbf{z}}$ Plane

Figure 6: Plots of RoI where ---- is the boundary $\|\mathbf{a}_1\|_2 = \|\mathbf{a}_2\|_2$, **- - -** is the boundary $V(\mathbf{r}_1, \mathbf{r}_2)$, $\triangle$ are the Lagrange points and $\circ$ is the asteroid

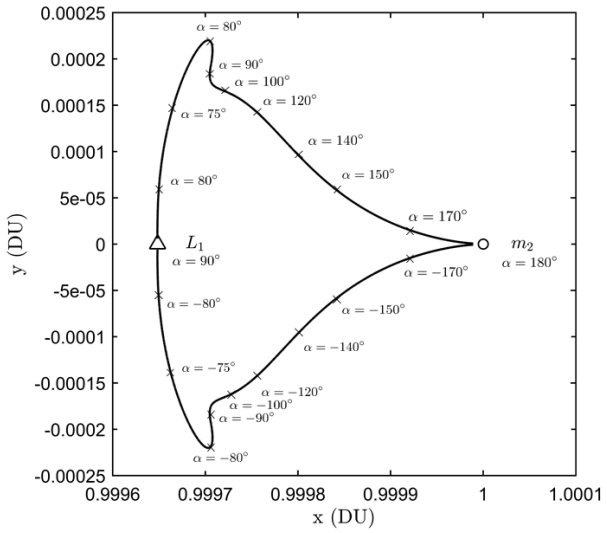

Figure 7: Solar sail equilibrium points for $\beta = 0.005$ and $\gamma = 90°$ with ARP in $\hat{\mathbf{x}} - \hat{\mathbf{y}}$ plane where — is the β contour, $\times$ are equilibrium points, $\triangle$ is L_1 Lagrange point and $\circ$ is the asteroid

$\hat{\mathbf{x}} - \hat{\mathbf{y}}$ plane and $\hat{\mathbf{x}} - \hat{\mathbf{z}}$ plane, respectively. Highlighted contours are the same $a : \beta = 0.0003$, $b : \beta = 0.0005$, $c : \beta = 0.005$, $d : \beta = 0.01$. The dashed boundary $S(\mathbf{r}_1, \mathbf{r}_2)$ distinguishes the shaded forbidden areas from the free areas where the β contours may not exist in the CR3BP model with SRP only due to $\mathbf{r}_1 \cdot \hat{\mathbf{n}} = 0$. $V(\mathbf{r}_1, \mathbf{r}_2)$ defines two disconnected shaded areas due to the constraint $\sum \mathbf{a} \cdot \hat{\mathbf{n}} \geq 0$ labelled as V_1 and V_2. This boundary shows where equilibrium solutions may not exist when both forces from SRP and ARP are included. The mass m_2 and the collinear Lagrange points L_1 and L_2, corresponding to the classical solutions with $\boldsymbol{\nabla} U = \mathbf{0}$ or $\alpha = 90°$ and $\psi = 0°$ lie on both of the boundaries. Without albedo effects the boundary reduces to $S(\mathbf{r}_1, \mathbf{r}_2)$ as shown in Figs. 3a and 3b. $\tilde{V}(\mathbf{r}_1, \mathbf{r}_2)$ is not shown in Figs. 5a and 5b, as the forbidden areas due to this constraint are infinitesimally small at m_2 and m_1 and did not appear in the simulations.

These results differ from Figs. 3a and 3b, showing that β contours in general have different shape due to the Lambertian BRDF. Noteworthy is that closer Sun-side equilibrium points exist between L_1 and m_2 which indicates induced beneficial effects on the solar sail in the current presented approximation for albedo effects. For flexible solar sail transfers then β has to be on

the smaller side. This means that the solar sail may move easily with smaller SRP force as, at some points, it would balance out the gravity and ARP, rendering existence of new equilibrium solutions. When $0.005 \leq \beta \leq \infty$, the contours do not change considerably. As $\beta \to \infty$, the equilibrium points approach the boundaries $S(\mathbf{r}_1, \mathbf{r}_2)$ and $V(\mathbf{r}_1, \mathbf{r}_2)$. The switching point is found to be at $\beta = 0.001$, where $\beta < 0.001$ give the conventional contours and $\beta > 0.001$ give the altered contours that asymptotically approach the boundary $V(\mathbf{r}_1, \mathbf{r}_2)$ as $\beta \to \infty$. It is emphasized again as shown in section 4 that the equilibrium points are still unstable but controllable in general.

It has been demonstrated that the β contours are nearly identical to the model with SRP only when in vicinity of L_1 and when outside the RoI or boundary $\|\mathbf{a}_1\|_2 = \|\mathbf{a}_2\|_2$. The RoI boundary is shown in Figs. 6a and 6b for the two planar cases. It is evident that in the vicinity of m_2 then $\|\mathbf{a}_1\|_2 < \|\mathbf{a}_2\|_2$, thus the solar sail will have equilibrium solutions also when $\hat{\mathbf{n}}$ is oriented towards the Sun, i.e. when incribed in the RoI interior to the boundary $S(\mathbf{r}_1, \mathbf{r}_2)$. The equilibrium points exactly at the RoI boundary are in theory found to be Lyapunov stable as claimed in section 4.

Fig. 7 explicitly shows a zoomed-in section of the equilibrium points for a constant $\beta = 0.005$ with $0^\circ \leq \alpha \leq 180^\circ$ for $\gamma = 0^\circ$ represented with the albedo value of $\rho = 0.2$. It can be explicitly seen that the attitude alone changes the position of the solar sail, and as $\alpha \to 180^\circ$ then the spacecraft will approach m_2 for the specific β chosen.

6. Conclusions

In this paper it is shown analytically and by analysis that adding ARP to SRP in the CR3BP significantly affects the solar sail dynamics as the artificial equilibrium points are shifted considerably for a Sun-minor body system. Artificial equilibrium points are found to exist on the Sun-side of the minor body, in a previously inadmissible volume for equilibrium points between the Lagrange point L_1 and the minor body, which enables novel opportunities for solar sails. Hovering locations for closer observations are possible in the vicinity of both L_1 and L_2 Lagrange points which may alleviate mission operations.

By analytical analysis of local stability it is found that the equilibrium points are unstable when ARP is included in the CR3BP. The equilibrium points found to be Lyapunov stable exactly at the RoI boundary. The system is found to be controllable in general for attitude angles as control inputs,

thus the solar sail may alter the orientation to enforce asymptotic stability or even Lyapunov stability at the points of interest. It can be concluded that linearization about the equilibrium points has to take the ARP forces into account in order to have a well-defined framework for solar sail control in the vicinity of a minor body with high albedo.

The findings are benificial for any spacecraft mission to distant planets, asteroids or comets. For an asteroid or comet it is also important to investigate other dominant perturbation effects. Future work may involve analysis of periodic orbits around the artificial on-axis and off-axis equilibrium points, transfers between equilibrium points, oblateness effects and elliptical models for both the Sun-minor body and Sun-Earth-minor body systems.

Battin, R. H., 1999. An Introduction to the Mathematics and Methods of Astrodynamics (Revised Edition). American Institute of Aeronautics and Astronautics.

Broschart, S. B., Scheeres, D. J., 2005. Control of Hovering Spacecraft Near Small Bodies: Application to Asteroid 25143 Itokawa. Journal of Guidance, Control, and Dynamics 28, 343–354.

Burns, J. A., Lamy, P. L., Soter, S., 1979. Radiation Forces on Small Particles in the Solar System. Icarus 40, 1–48.

Busch, M. W., Benner, L. A. M., Ostro, S. J., Giorgini, J. D., Jurgens, R. F., Rose, R., Scheeres, D. J., Magri, C., Margot, J., Nolan, M. C., Hine, A. A., 2008. Physical properties of a near-Earth Asteroid (33342) 1998 WT24. Icarus 195, 614–621.

Ershkov, S. V., 2012. The Yarkovsky Effect in Generalized Photogravitational 3-Body Problem. Planetary and Space Science 73, 221–223.

Farquhar, R. W., Kamel, A. A., 1973. Quasi-Periodic Orbits About the Translunar Libration Point. Celestial Mechanics 7, 458–473.

Farres, A., Jorba, A., 2012. Station Keeping of a Solar Sail around a Halo Orbit. Acta Astronautica 94, 527–539.

Fernandez, Y. R., Jewitt, D. C., Sheppard, S. S., 2005. Albedos of Asteroids in Comet-Like Orbits. The Astronomical Journal 130, 308–318.

Hand, E., 2015. Dawn probe to look for a habitable ocean on Ceres. Science 347 (6224), 813–814.

Heiligers, J., McInnes, C. R., 2014. Novel Solar Sail Mission Concepts for Space Weather Forecasting. In: 24th AAS/AIAA Space Flight Mechanics Meeting 2014. No. AAS 14-239.

Hexi, B., McInnes, C. R., 2005. Solar Sail Orbits at Artificial SunEarth Libration Points. Journal of Guidance, Control and Dynamics 28 (6), 1328–1331.

Howell, K. C., 1984. Three-Dimensional, Periodic, 'Halo' Orbits. Celestial Mechanics 32, 53–71.

Kaasalainen, M., Torppa, J., Piironen, J., 2002. Models of Twenty Asteroids from Photometric Data. Icarus 159, 369–395.

Krag, W. E., September 1974. Visible Magnitude of Typical Satellites in Synchronous Orbits. Tech. Rep. ESD-TR-74-278, Massachusets Institute of Technology.

Macdonald, M., McInnes, C. R., 2011. Solar Sail Science Mission Applications and Advancement. Advances in Space Research 48, 1702–1716.

Magnusson, P., Dahlgren, M., Barucci, M. A., Jorda, L., Binzel, R. P., Slivan, S. M., Blanco, C., Riccioli, D., Buratti, B. J., Colas, F., Berthier, J., Angelis, G. D., Martino, M. D., Dotto, E., Drummond, J. D., Fink, U., Hicks, M., Grundy, W., Wisniewski, W., Gaftonyuk, N. M., Geyer, E. H., Bauer, T., Hoffmann, M., Ivanova, V., Komitov, B., Donchev, Z., Denchev, P., Krugly, Y. N., Velichko, F. P., Chiorny, V. G., Lupishko, D. F., Shevchenko, V. G., Kwiatkowski, T., Kryszczynska, A., Lahulla, J. F., Licandro, J., Mendez, O., Mottola, S., Erikson, A., Ostro, S. J., Pravec, P., Pych, W., Tholen, D. J., Whiteley, R., Wild, W. J., Wolf, M., Sarounova, L., September 1996. Photometric Observations and Modeling of Asteroids 1620 Geographos. Icarus 123 (1), 227–244.

McInnes, A. I. S., 2000. Strategies for Solar Sail Mission Design in the Circular Restricted Three-Body Problem. Master's thesis, Purdue University.

McInnes, C. R., 1999. Solar Sailing: Technology, Dynamics and Mission Applications. Springer Praxis.

McInnes, C. R., McDonald, A. J. C., Simmons, J. F. L., 1994. Solar Sail Parking in Restricted Three-Body Systems. Journal of Guidance, Control, and Dynamics.

Michel, P., Yoshikawa, M., 2005. Earth Impact Probability of the Asteroid (25143) Itokawa to be Sampled by the Spacecraft Hayabusa. Icarus 179, 291–296.

Morrow, E., Scheeres, D. J., Lubin, D., 2001. Solar Sail Orbit Operations at Asteroids. Journal of Spacecraft and Rockets 38, 279–286.

Nesvorny, D., Bottke, W. F., Levison, H. F., Dones, L., 2003. Recent Origin of the Solar System Dust Bands. The Astrophysical Journal 591 (1), 486–497.

Nuss, J. S., 1998. The Use of Solar Sail in the Circular Restricted Problem of Three Bodies. Master's thesis, Purdue University.

Scheeres, D. J., Abe, M., Yoshikawa, M., Nakamura, R., Gaskell, R. W., Abell, P. A., 2007. The Effect of YORP on Itokawa. Icarus 188, 425–429.

Scheeres, D. J., Marzari, F., 2002. Spacecraft Dynamics in the Vicinity of a Comet. Journal of the Astronautical Sciences 50(1), 35–52.

Shell, J. R., 2010. Optimizing Orbital Debris Monitoring with Optical Telescopes. Tech. rep., US Air Force, Space Innovation and Development Center.

Sonter, M. J., 1997. The Technical and Economic Feasibility of Mining the Near-Earth Asteroids. Acta Astronautica 41, 637–647.

Taylor, M. G. G. T., Alexander, C., Altobelli, N., Fulle, M., Fulchignoni, M., Grün, E., Weissman, P., 2015. Rosetta begins its comet tale. Science 347 (6220), 387–387.

Tsuda, Y., Mori, O., Funase, R., Sawada, H., Yamamoto, T., Saiki, T., Endo, T., Yonekura, K., Hoshino, H., Kawaguchi, J., February 2013. Achievement of IKAROS - Japanese Deep Space Solar Sail Demonstration Mission. Acta Astronautica 82 (2), 183–188.

Appendix A. Background

The following content describes the derivations and results based on previous work in McInnes et al. (1994); McInnes (1999) and includes only solar radiation pressure in the solar sail circular restricted three body problem (CR3BP).

In the CR3BP, both the large and minor primary objects are treated as point masses denoted as m_1 and m_2, respectively, and the satellite mass m_3 is assumed to be infinitesimally small. The relative sizes are denoted as $m_1 > m_2 >> m_3$. The objects revolve around a common center of mass which defines the rotating reference frame $\mathcal{B}$: $\{\hat{\mathbf{x}}, \hat{\mathbf{y}}, \hat{\mathbf{z}}\}$ rotating with an angular velocity $\boldsymbol{\omega}_{\mathcal{B}/\mathcal{I}}$ with respect to the inertial frame $\mathcal{I}$: $\{\hat{\mathbf{i}}_1, \hat{\mathbf{i}}_2, \hat{\mathbf{i}}_3\}$. The dimensions are normalized such that the distance between the primary masses r_{12}, the sum of primary masses $m_1 + m_2$ and the gravitational constant G are all defined to be unity. The mass ratio of the system is defined as $\mu = m_2/(m_1 + m_2)$. The frame rotates once about the $\hat{\mathbf{z}}$-axis in $2\pi/\omega$ time units. By definition, the angular velocity $\boldsymbol{\omega}_{\mathcal{B}/\mathcal{I}}$ is equal to the mean motion and has also a nondimensional magnitude equal to unity. $\boldsymbol{\omega}_{\mathcal{B}/\mathcal{I}}$ may be expressed as

$$\boldsymbol{\omega}_{\mathcal{B}/\mathcal{I}} = \boldsymbol{\omega} = \hat{\mathbf{z}} \tag{A.1}$$

The position vectors for the solar sail with respect to m_1 and m_2 in the rotating frame, as seen in Fig. 1, are defined as

$$\begin{aligned} \mathbf{r}_1 &= [(x + \mu)\ y\ z]^T \\ \mathbf{r}_2 &= [(x - (1 - \mu))\ y\ z]^T \end{aligned} \tag{A.2}$$

In general the total force exerted on the solar sail is expressed as

$$\sum \mathbf{F} = \mathbf{F}_g + \mathbf{F}_{SRP} + \mathbf{F}_{other} \tag{A.3}$$

However if $\mathbf{F}_{other}$ can be neglected, then the SRP force $\mathbf{F}_{SRP}$ is the only force that needs to be considered and can be analyzed separately from the gravitational force $\mathbf{F}_g$. SRP is assumed to act on only one surface of the solar sail. The detailed physics of SRP acting on a perfectly reflecting flat plate are discussed in McInnes (1999). The expression for radiation pressure is as follows

$$P = \frac{W}{c} \tag{A.4}$$

where P is the magnitude of the radiation pressure force, c is the speed of light and W represents the energy flux of the electromagnetic radiation that creates pressure. Assuming the Sun can be modelled as a point source, the energy flux varies proportionally with the inverse square of the distance from the Sun. W can be written in terms of the solar luminosity $\mathfrak{L}_1$ and scaled by the Sun-Earth distance R_E as

$$W = W_E \left(\frac{R_E}{r_1} \right)^2$$
$$W_E = \frac{\mathfrak{L}_1}{4\pi R_E^2}$$

where W_E is the mean energy flux measured at the Earth's distance from the Sun, generally taken to be $1368 \mathrm{Js}^{-1}\mathrm{m}^{-2}$ at 1AU. The solar sail intercepts

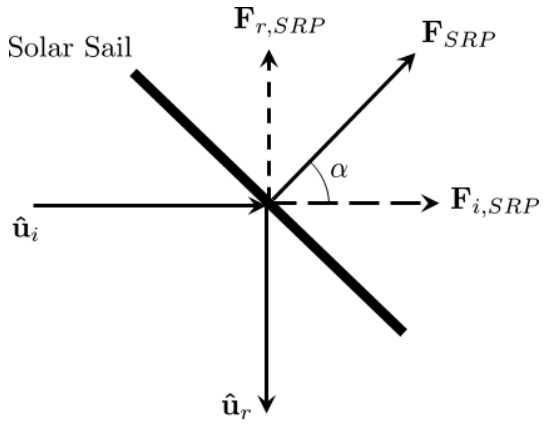

Figure A.1: SRP force exerted on a perfectly reflecting solar sail

photons of all possible frequencies, and reflect them in perfectly elastic collisions. Therefore the momentum transfer force from incident photons creates a reaction force of equal magnitude from the reflected photons. A solar sail is an oriented surface such that the acceleration of the solar sail is a function of the sail attitude. For a sail area A with unit vector $\hat{\mathbf{n}}$ with direction normal to the sail surface, the SRP force exerted on the sail due to photons incident from $\hat{\mathbf{u}}_i$ direction is given by

$$\mathbf{F}_{i,SRP} = PA(\hat{\mathbf{u}}_i \cdot \hat{\mathbf{n}})\hat{\mathbf{u}}_i \tag{A.5}$$

where $A(\hat{\mathbf{u}}_i \cdot \hat{\mathbf{n}})$ is the projected sail area in the $\hat{\mathbf{u}}_i$ direction. Fig. A.1 shows a schematic of the physics acting on the solar sail. By Newton's Third Law, the reflected photons will exert a force of equal magnitude on the solar sail, but in the specular reflected direction $-\hat{\mathbf{u}}_r$, i.e.

$$\mathbf{F}_{r,SRP} = -PA(\hat{\mathbf{u}}_i \cdot \hat{\mathbf{n}})\hat{\mathbf{u}}_r \tag{A.6}$$

Since $\hat{\mathbf{u}}_i - \hat{\mathbf{u}}_r = 2(\hat{\mathbf{u}}_i \cdot \hat{\mathbf{n}})\hat{\mathbf{n}}$, the total force $\mathbf{F}_{SRP}$ is then given by

$$\mathbf{F}_{SRP} = 2PA(\hat{\mathbf{u}}_i \cdot \hat{\mathbf{n}})^2\hat{\mathbf{n}} \tag{A.7}$$

or

$$\mathbf{F}_{SRP} = \frac{2AW}{c}(\hat{\mathbf{u}}_i \cdot \hat{\mathbf{n}})^2\hat{\mathbf{n}} \tag{A.8}$$

Using Eq. (A.5), then the force may be expressed as

$$\mathbf{F}_{SRP} = \frac{2AW_E}{c}\left(\frac{R_E}{r_1}\right)^2(\hat{\mathbf{u}}_i \cdot \hat{\mathbf{n}})^2\hat{\mathbf{n}} \tag{A.9}$$

or

$$\mathbf{F}_{SRP} = \frac{A\mathfrak{L}_1}{2\pi c r_1^2}(\hat{\mathbf{u}}_i \cdot \hat{\mathbf{n}})^2\hat{\mathbf{n}} \tag{A.10}$$

As shown in Fig. (A.1), the sail pitch angle α may be expressed as the angle between the normal vector or sail attitude vector $\hat{\mathbf{n}}$ and the incident radiation vector $\hat{\mathbf{u}}_i$. Thus the acceleration due to radiation pressure may be expressed as

$$\mathbf{a}_1 = \frac{\mathfrak{L}_1}{2\pi c\sigma r_1^2}\cos^2\alpha\hat{\mathbf{n}} \tag{A.11}$$

where the solar sail performance may be parametrized by the total spacecraft mass per unit area m_3/A or commonly known as sail loading σ. For a solar sail in heliocentric orbit the direction of incidence of radiation $\hat{\mathbf{u}}_i$ is defined by the unit vector $\hat{\mathbf{r}}_1$. Then the acceleration exerted on the solar sail may be expressed as

$$\mathbf{a}_1 = \beta\frac{Gm_1}{r_1^2}\langle\hat{\mathbf{r}}_1 \cdot \hat{\mathbf{n}}\rangle^2\hat{\mathbf{n}} \tag{A.12}$$

or in nondimensionalized form in a CR3BP system

$$\mathbf{a}_1 = \beta\frac{(1-\mu)}{r_1^2}\langle\hat{\mathbf{r}}_1 \cdot \hat{\mathbf{n}}\rangle^2\hat{\mathbf{n}} \tag{A.13}$$

Knowing that $\hat{\mathbf{r}}_1$ is directed along the Sun-line and since the SRP force can never be directed sunwards, the solar sail orientation is constrained to be nonnegative (McInnes et al., 1994). Therefore the $\langle \cdot \rangle$ term is the nonnegative operator i.e.

$$\langle x \rangle = \begin{cases} x & \text{if } x \geq 0 \\ 0 & \text{if } x < 0 \end{cases}$$

The dimensionless sail loading parameter β is the defined as the ratio of the radiation pressure force to the solar gravitational force exerted on the sail, otherwise known as the lightness number of the solar sail (McInnes et al., 1994). This may be expressed as

$$\beta = \frac{\sigma^*}{\sigma} \tag{A.14}$$

where

$$\sigma^* = \frac{\mathfrak{L}_1}{2\pi G m_1 c} \tag{A.15}$$

where $\mathfrak{L}_1$ is the luminosity of the large primary object, where for the Sun it is taken to be approximately $3.846 \times 10^{26}\ W$. It is easy to see that a large β is induced by large A/m_3 ratio, that means the larger the sail area is compared to the mass, then the sail will experience higher acceleration $\mathbf{a}_1$. On the other hand, the sail will have smaller β if area is smaller with fixed spacecraft mass. Acceleration $\mathbf{a}_1$ is also highly dependent on the sail orientation defined by the $\langle \cdot \rangle$ term.

The reduced vector form of equations of motion (EoM) for a solar sail with $\mathbf{r}$ being the vector from the center of mass to m_3 can be defined in the rotating frame as (McInnes et al., 1994)

$$\ddot{\mathbf{r}} + 2\boldsymbol{\omega} \times \dot{\mathbf{r}} + \boldsymbol{\nabla} U = \mathbf{a}_1 \tag{A.16}$$

The state space form of the solar sail EoM may be written as a nonlinear time-invariant vector differential equation

$$\begin{bmatrix} \dot{\mathbf{r}} \\ \ddot{\mathbf{r}} \end{bmatrix} = \begin{bmatrix} \mathbf{f}_1(\mathbf{r}, \mathbf{u}) \\ \mathbf{f}_2(\mathbf{r}, \mathbf{u}) \end{bmatrix} \tag{A.17}$$

Based on the EoM this is written in explicit form as

$$\begin{bmatrix} \dot{\mathbf{r}} \\ \ddot{\mathbf{r}} \end{bmatrix} = \begin{bmatrix} \dot{\mathbf{r}} \\ \mathbf{a}_1 - \boldsymbol{\nabla} U - 2\boldsymbol{\omega} \times \dot{\mathbf{r}} \end{bmatrix} \tag{A.18}$$

At equilibrium $\mathbf{r} = \mathbf{r}^*$ then $\dot{\mathbf{r}} = \mathbf{0}$ i.e. $\mathbf{f}_1(\mathbf{r}, \mathbf{u}) = \mathbf{0}$ and $\ddot{\mathbf{r}} = \mathbf{0}$. Thus

$$\mathbf{0} = \begin{bmatrix} \mathbf{0} \\ \mathbf{a}_1 - \boldsymbol{\nabla} U \end{bmatrix} \tag{A.19}$$

In scalar form the three body potential U may be written as

$$U = -\left(\frac{1}{2}(x^2 + y^2) + \frac{1-\mu}{r_1} + \frac{\mu}{r_2} \right) \tag{A.20}$$

Stationary solutions require condition in Eq. (A.19). Then, with $\hat{\mathbf{n}}$ being oriented in the direction of $\mathbf{a}_1$, taking the cross product of $\hat{\mathbf{n}}$ with Eq. (**??**), it follows that

$$\boldsymbol{\nabla} U \times \hat{\mathbf{n}} = 0 \Rightarrow \hat{\mathbf{n}} = \epsilon \boldsymbol{\nabla} U \tag{A.21}$$

where ϵ is an arbitrary scalar multiplier. Using the fact that $\|\hat{\mathbf{n}}\|_2 = 1$, then $\epsilon = \|\boldsymbol{\nabla} U\|_2^{-1}$, therefore requiring a stationary solution, then

$$\hat{\mathbf{n}} = \frac{\boldsymbol{\nabla} U}{\|\boldsymbol{\nabla} U\|_2} \tag{A.22}$$

$$\boldsymbol{\nabla} U = \begin{bmatrix} U_x \\ U_y \\ U_z \end{bmatrix} = \begin{bmatrix} -x + \frac{(1-\mu)(x+\mu)}{r_1^3} + \frac{\mu(x-(1-\mu))}{r_2^3} \\ -y + \frac{(1-\mu)y}{r_1^3} + \frac{\mu y}{r_2^3} \\ \frac{(1-\mu)z}{r_1^3} + \frac{\mu z}{r_2^3} \end{bmatrix} \tag{A.23}$$

With $\boldsymbol{\nabla} U = \mathbf{0}$ the five classical equilibrium points at $\mathbf{r}_{L_i}, i = (1, ..., 5)$ can be found as the system is reduced to the conventional CR3BP. However, when including solar sail acceleration $\mathbf{a}_1$ then new artificial equilibrium solutions emerge.

The sail cone (pitch) angle, α and clock (precession) angle, γ, define the sail attitude with respect to the coordinate system $\mathcal{R}$: $\{\hat{\mathbf{r}}_1, \hat{\mathbf{r}}_1 \times \hat{\mathbf{z}}, (\hat{\mathbf{r}}_1 \times \hat{\mathbf{z}}) \times \hat{\mathbf{r}}_1\}$ located on the solar sail center of mass. The pitch angle α controls the magnitude of the radiation pressure force and the clock angle controls the force direction. A schematic is shown in Fig. A.2. The angles may be written

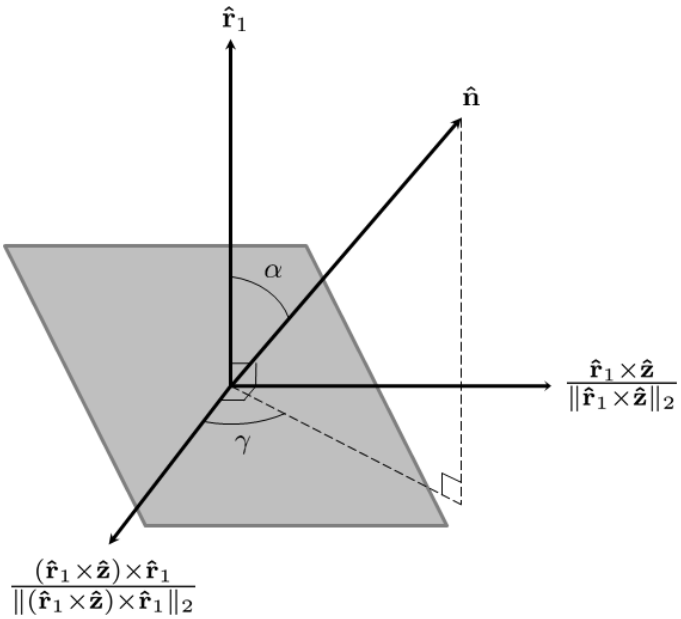

Figure A.2: Schematic of solar sail cone and clock angles

as

$$\tan\alpha = \frac{\|\hat{\mathbf{r}}_1 \times \boldsymbol{\nabla} U\|_2}{\hat{\mathbf{r}}_1 \cdot \boldsymbol{\nabla} U} \tag{A.24}$$

$$\tan\gamma = \frac{\|((\hat{\mathbf{r}}_1 \times \hat{\mathbf{z}}) \times \hat{\mathbf{r}}_1) \times (\hat{\mathbf{r}}_1 \times \boldsymbol{\nabla} U)\|_2}{((\hat{\mathbf{r}}_1 \times \hat{\mathbf{z}}) \times \hat{\mathbf{r}}_1) \cdot (\hat{\mathbf{r}}_1 \times \boldsymbol{\nabla} U)} \tag{A.25}$$

The sail attitude with respect to $\mathbf{r}_2$ can be defined as $(\psi - \alpha)$, and from using trigonometric identities then

$$\begin{aligned} \tan(\psi - \alpha) =& \frac{\|\hat{\mathbf{r}}_2 \times \boldsymbol{\nabla} U\|_2}{\hat{\mathbf{r}}_2 \cdot \boldsymbol{\nabla} U} \\ =& \frac{(\|\hat{\mathbf{r}}_1 \times \hat{\mathbf{r}}_2\|_2)(\hat{\mathbf{r}}_1 \cdot \boldsymbol{\nabla} U) - (\hat{\mathbf{r}}_1 \cdot \hat{\mathbf{r}}_2)(\|\hat{\mathbf{r}}_1 \times \boldsymbol{\nabla} U\|_2)}{(\hat{\mathbf{r}}_1 \cdot \hat{\mathbf{r}}_2)(\hat{\mathbf{r}}_1 \cdot \boldsymbol{\nabla} U) + (\|\hat{\mathbf{r}}_1 \times \hat{\mathbf{r}}_2\|_2)(\|\hat{\mathbf{r}}_1 \times \boldsymbol{\nabla} U\|_2)} \end{aligned} \tag{A.26}$$

The solar sail orientation can be expressed in terms of the components of $\hat{\mathbf{n}}$ with respect to the rotating frame (McInnes, 2000). The scalar components of $\hat{\mathbf{n}}$ corresponding to the directions $\hat{\mathbf{x}}$, $\hat{\mathbf{y}}$, $\hat{\mathbf{z}}$ are

$$n_x = \frac{\cos\alpha(x+\mu)}{r_1} - \frac{\sin\alpha\cos\gamma(x+\mu)z}{\|(\mathbf{r}_1 \times \hat{\mathbf{z}}) \times \mathbf{r}_1\|_2} + \frac{\sin\alpha\sin\gamma y}{\|\mathbf{r}_1 \times \hat{\mathbf{z}}\|_2} \tag{A.27}$$

$$n_y = \frac{\cos\alpha y}{r_1} - \frac{\sin\alpha\cos\gamma yz}{\|(\mathbf{r}_1 \times \hat{\mathbf{z}}) \times \mathbf{r}_1\|_2} - \frac{\sin\alpha\sin\gamma(x+\mu)}{\|\mathbf{r}_1 \times \hat{\mathbf{z}}\|_2} \tag{A.28}$$

$$n_z = \frac{\cos\alpha z}{r_1} - \frac{\sin\alpha\cos\gamma(y^2 + (x+\mu)^2)}{\|(\mathbf{r}_1 \times \hat{\mathbf{z}}) \times \mathbf{r}_1\|_2} \tag{A.29}$$

where

$$\|\mathbf{r}_1\|_2 = r_1 = \sqrt{(x+\mu)^2 + y^2 + z^2}, \tag{A.30}$$

$$\|\mathbf{r}_1 \times \hat{\mathbf{z}}\|_2 = \sqrt{(x+\mu)^2 + y^2}, \tag{A.31}$$

$$\|(\mathbf{r}_1 \times \hat{\mathbf{z}}) \times \mathbf{r}_1\|_2 = \sqrt{(x+\mu)^2 z^2 + y^2 z^2 + ((x+\mu)^2 + y^2)^2}, \tag{A.32}$$

With the solar sail orientation angles defined, then the effects of a solar sail may be added to the scalar EoM in the CR3BP. The solar sail acceleration may be expressed in scalar components with respect to rotating coordinates as

$$a_{1,x} = \beta\frac{(1-\mu)}{r_1^2}\cos^2\alpha n_x \tag{A.33}$$

$$a_{1,y} = \beta\frac{(1-\mu)}{r_1^2}\cos^2\alpha n_y \tag{A.34}$$

$$a_{1,z} = \beta\frac{(1-\mu)}{r_1^2}\cos^2\alpha n_z \tag{A.35}$$

Thus the compact scalar form of solar sail EoM added with SRP are of the form

$$\ddot{x} - 2\dot{y} = -U_x + a_{1,x} \tag{A.36}$$

$$\ddot{y} + 2\dot{x} = -U_y + a_{1,y} \tag{A.38}$$

$$\ddot{z} = -U_z + a_{1,z} \tag{A.37}$$

Equilibrium solutions are created when the left hand terms are zero, or equivalently when the SRP acceleration balances the gravitational acceleration, i.e. $\boldsymbol{\nabla} U = \mathbf{a}_1$. Evaluating Eq. (A.20) and taking the scalar product of Eq. (A.19) with $\hat{\mathbf{n}}$, and requiring to be at equilibrium solutions, the solar lightness number may be expressed as

$$\beta = \frac{r_1^2}{(1-\mu)}\frac{\boldsymbol{\nabla} U \cdot \hat{\mathbf{n}}}{\langle \hat{\mathbf{r}}_1 \cdot \hat{\mathbf{n}} \rangle^2} \tag{A.38}$$

The classical solutions without solar sail correspond to the subset $\beta = 0$.

With $\beta > 0$ a particular equilibrium solution on a given surface is defined by the sail cone and clock attitude angles in Eq. (A.24) and Eq. (A.25).

Evaluating the gradient of the potential U for the condition $\hat{\mathbf{r}}_1 \cdot \hat{\mathbf{n}} = 0$ or equivalently $\hat{\mathbf{r}}_1 \cdot \boldsymbol{\nabla} U = 0$, as a result of $\hat{\mathbf{n}}$ being defined in Eq. (A.22), a function $S(\mathbf{r}_1, \mathbf{r}_2) = 0$ is obtained as follows

$$
\begin{aligned}
\mathbf{r}_1 \cdot \boldsymbol{\nabla} U =& [(x+\mu)\ y\ z] \cdot \begin{bmatrix} -x + \frac{(1-\mu)(x+\mu)}{r_1^3} + \frac{\mu(x-(1-\mu))}{r_2^3} \\ -y + \frac{(1-\mu)y}{r_1^3} + \frac{\mu y}{r_2^3} \\ \frac{(1-\mu)z}{r_1^3} + \frac{\mu z}{r_2^3} \end{bmatrix} \\
=& -x(x+\mu) + \frac{(1-\mu)(x+\mu)^2}{r_1^3} + \frac{\mu(x-(1-\mu))(x+\mu)}{r_2^3} \\
& - y^2 + \frac{(1-\mu)y^2}{r_1^3} + \frac{\mu(x-(1-\mu))y^2}{r_2^3} + \frac{(1-\mu)z^2}{r_1^3} \\
& + \frac{\mu(x-(1-\mu))z^2}{r_2^3} \\
=& -x(x+\mu) - y^2 + \frac{(1-\mu)}{r_1^3}\left((x+\mu)^2 + y^2 + z^2\right) \\
& \frac{\mu}{r_2^3}\left((x-(1-\mu))(x+\mu) + y^2 + z^2\right) \\
=& -x(x+\mu) - y^2 + \frac{(1-\mu)r_1^2}{r_1^3} + \frac{\mu \mathbf{r}_1 \cdot \mathbf{r}_2}{r_2^3} = 0 \\
\Rightarrow S =& x(x+\mu) + y^2 - \frac{1-\mu}{r_1} - \mu \frac{\mathbf{r}_1 \cdot \mathbf{r}_2}{r_2^3}
\end{aligned}
\tag{A.39}
$$

which defines regions where the solutions may exist and creates two topologically disconnected boundary surfaces. Not only do the five classical Lagrange points lie on these surfaces since they are solutions to $\boldsymbol{\nabla} U = \mathbf{0}$ but, in general, the sail loading surfaces also approach the boundary asymptotically as $\beta \to \infty$ since $\hat{\mathbf{r}}_1 \cdot \boldsymbol{\nabla} U \to 0$. It can easily be seen that $S(\mathbf{r}_1, \mathbf{r}_2)$ does not explicitly depend on SRP, but it depends on the sail position. In the free areas the equilibrium points indicate that the solar sail is in tension between SRP and gravitational forces but in forbidden areas this may not happen and one force dominates the other for any orientation or solar sail lightness number.

Appendix B. Second Partial Derivatives of the On-Axis Pseudo-Potential

The scalar expressions for the second partial derivatives of the pseudo-potential U are given here.

$$U_{xx} = 1 - \frac{1-\mu}{r_1^3} - \frac{\mu}{r_2^3} + \frac{3(1-\mu)(x+\mu)^2}{r_1^5} + \frac{3\mu(x-(1-\mu))^2}{r_2^5} \tag{B.1}$$

$$U_{xy} = \frac{3(1-\mu)(x+\mu)y}{r_1^5} + \frac{3\mu(x-(1-\mu))y}{r_2^5} \tag{B.2}$$

$$U_{xz} = \frac{3(1-\mu)(x+\mu)z}{r_1^5} + \frac{3\mu(x-(1-\mu))z}{r_2^5} \tag{B.3}$$

$$U_{yx} = \frac{3(1-\mu)(x+\mu)y}{r_1^5} + \frac{3\mu(x-(1-\mu))y}{r_2^5} \tag{B.4}$$

$$U_{yy} = 1 - \frac{1-\mu}{r_1^3} - \frac{\mu}{r_2^3} + \frac{3(1-\mu)y^2}{r_1^5} + \frac{3\mu y^2}{r_2^5} \tag{B.5}$$

$$U_{yz} = \frac{3(1-\mu)yz}{r_1^5} + \frac{3\mu yz}{r_2^5} \tag{B.6}$$

$$U_{zx} = \frac{3(1-\mu)(x+\mu)z}{r_1^5} + \frac{3\mu(x-(1-\mu))z}{r_2^5} \tag{B.7}$$

$$U_{zy} = \frac{3(1-\mu)yz}{r_1^5} + \frac{3\mu yz}{r_2^5} \tag{B.8}$$

$$U_{zz} = -\frac{1-\mu}{r_1^3} - \frac{\mu}{r_2^3} + \frac{3(1-\mu)z^2}{r_1^5} + \frac{3\mu z^2}{r_2^5} \tag{B.9}$$

Appendix C. Partial Derivatives of the Solar Sail SRP Acceleration Terms Relative to Position

The scalar expressions for the second partial derivatives of the solar sail acceleration $\mathbf{a}_1$ with respect to position (assumed that solar sail cone and clock angles, α and γ, are independent of position) are given here.

$$\begin{aligned} a_{1,xx} =&\beta\frac{(1-\mu)}{r_1^2}\cos^2\alpha\bigg(-\frac{2(x+\mu)n_x}{r_1^2}+\frac{\cos\alpha(y^2+z^2)}{r_1^3} \\ &-\frac{\sin\alpha\sin\gamma y(x+\mu)}{\|\mathbf{r}_1\times\hat{\mathbf{z}}\|_2^3}+\frac{\sin\alpha\cos\gamma z((x+\mu)^4-y^2z^2-y^4)}{\|(\mathbf{r}_1\times\hat{\mathbf{z}})\times\mathbf{r}_1\|_2^3}\bigg) \end{aligned} \tag{C.1}$$

$$\begin{aligned} a_{1,xy} =&\beta\frac{(1-\mu)}{r_1^2}\cos^2\alpha\bigg(-\frac{2yn_x}{r_1^2}-\frac{\cos\alpha(x+\mu)y}{r_1^3}+\frac{\sin\alpha\sin\gamma(x+\mu)^2}{\|\mathbf{r}_1\times\hat{\mathbf{z}}\|_2^3} \\ &+\frac{\sin\alpha\cos\gamma(x+\mu)yz(2(x+\mu)^2+2y^2+z^2)}{\|(\mathbf{r}_1\times\hat{\mathbf{z}})\times\mathbf{r}_1\|_2^3}\bigg) \end{aligned} \tag{C.2}$$

$$\begin{aligned} a_{1,xz} =&\beta\frac{(1-\mu)}{r_1^2}\cos^2\alpha\bigg(-\frac{2zn_x}{r_1^2}-\frac{\cos\alpha(x+\mu)z}{r_1^3} \\ &-\frac{\sin\alpha\cos\gamma(x+\mu)((x+\mu)^2+y^2)^2}{\|(\mathbf{r}_1\times\hat{\mathbf{z}})\times\mathbf{r}_1\|_2^3}\bigg) \end{aligned} \tag{C.3}$$

$$\begin{aligned} a_{1,yx} =&\beta\frac{(1-\mu)}{r_1^2}\cos^2\alpha\bigg(-\frac{2(x+\mu)n_y}{r_1^2}-\frac{\cos\alpha(x+\mu)y}{r_1^3}-\frac{\sin\alpha\sin\gamma y^2}{\|\mathbf{r}_1\times\hat{\mathbf{z}}\|_2^3} \\ &+\frac{\sin\alpha\cos\gamma(x+\mu)yz(2(x+\mu)^2+2y^2+z^2)}{\|(\mathbf{r}_1\times\hat{\mathbf{z}})\times\mathbf{r}_1\|_2^3}\bigg) \end{aligned} \tag{C.4}$$

$$\begin{aligned} a_{1,yy} =&\beta\frac{(1-\mu)}{r_1^2}\cos^2\alpha\bigg(-\frac{2yn_y}{r_1^2}+\frac{\cos\alpha((x+\mu)^2+z^2)}{r_1^3} \\ &+\frac{\sin\alpha\sin\gamma y^2}{\|\mathbf{r}_1\times\hat{\mathbf{z}}\|_2^3}-\frac{\sin\alpha\cos\gamma z((x+\mu)^2(z^2+(x+\mu)^2)-y^4)}{\|(\mathbf{r}_1\times\hat{\mathbf{z}})\times\mathbf{r}_1\|_2^3}\bigg) \end{aligned} \tag{C.5}$$

$$a_{1,yz} = \beta \frac{(1-\mu)}{r_1^2} \cos^2\alpha \Bigg(-\frac{2zn_y}{r_1^2} - \frac{\cos\alpha zy}{r_1^3} - \frac{\sin\alpha\cos\gamma y((x+\mu)^2+y^2)^2}{\|(\mathbf{r}_1 \times \hat{\mathbf{z}}) \times \mathbf{r}_1\|_2^3} \Bigg) \tag{C.6}$$

$$a_{1,zx} = \beta \frac{(1-\mu)}{r_1^2} \cos^2\alpha \Bigg(-\frac{2(x+\mu)n_z}{r_1^2} - \frac{\cos\alpha(x+\mu)z}{r_1^3} + \frac{\sin\alpha\cos\gamma(x+\mu)z^2((x+\mu)^2+y^2)}{\|(\mathbf{r}_1 \times \hat{\mathbf{z}}) \times \mathbf{r}_1\|_2^3} \Bigg) \tag{C.7}$$

$$a_{1,zy} = \beta \frac{(1-\mu)}{r_1^2} \cos^2\alpha \Bigg(-\frac{2yn_z}{r_1^2} - \frac{\cos\alpha yz}{r_1^3} + \frac{\sin\alpha\cos\gamma yz^2((x+\mu)^2+y^2)}{\|(\mathbf{r}_1 \times \hat{\mathbf{z}}) \times \mathbf{r}_1\|_2^3} \Bigg) \tag{C.8}$$

$$a_{1,zz} = \beta \frac{(1-\mu)}{r_1^2} \cos^2\alpha \Bigg(-\frac{2zn_z}{r_1^2} + \frac{\cos\alpha((x+\mu)^2+y^2)}{r_1^3} - \frac{\sin\alpha\cos\gamma z((x+\mu)^2+y^2)^2}{\|(\mathbf{r}_1 \times \hat{\mathbf{z}}) \times \mathbf{r}_1\|_2^3} \Bigg) \tag{C.9}$$

Appendix D. Partial Derivatives of the Solar Sail ARP Acceleration Terms Relative to Position

The scalar expressions for the second partial derivatives of the solar sail acceleration $\mathbf{a}_2$ with respect to position (assumed that solar sail cone and clock angles, α and γ, are independent of position) are given here.

$$\begin{aligned} a_{2,xx} =&\beta\frac{(1-\mu)d_2^2\rho p(\phi)}{r_2^4}\cos^2(\psi-\alpha)\bigg(-\frac{4(x-1+\mu)n_x}{r_2^2} \\ &+\frac{\cos\alpha(y^2+z^2)}{r_1^3}-\frac{\sin\alpha\sin\gamma y(x+\mu)}{\|\mathbf{r}_1\times\hat{\mathbf{z}}\|_2^3} \\ &+\frac{\sin\alpha\cos\gamma z((x+\mu)^4-y^2z^2-y^4)}{\|(\mathbf{r}_1\times\hat{\mathbf{z}})\times\mathbf{r}_1\|_2^3}\bigg) \end{aligned} \tag{D.1}$$

$$\begin{aligned} a_{2,xy} =&\beta\frac{(1-\mu)d_2^2\rho p(\phi)}{r_2^4}\cos^2(\psi-\alpha)\bigg(-\frac{4yn_x}{r_2^2}-\frac{\cos\alpha(x+\mu)y}{r_1^3} \\ &+\frac{\sin\alpha\sin\gamma(x+\mu)^2}{\|\mathbf{r}_1\times\hat{\mathbf{z}}\|_2^3} \\ &+\frac{\sin\alpha\cos\gamma(x+\mu)yz(2(x+\mu)^2+2y^2+z^2)}{\|(\mathbf{r}_1\times\hat{\mathbf{z}})\times\mathbf{r}_1\|_2^3}\bigg) \end{aligned} \tag{D.2}$$

$$\begin{aligned} a_{2,xz} =&\beta\frac{(1-\mu)d_2^2\rho p(\phi)}{r_2^4}\cos^2(\psi-\alpha)\bigg(-\frac{4zn_x}{r_2^2}-\frac{\cos\alpha(x+\mu)z}{r_1^3} \\ &-\frac{\sin\alpha\cos\gamma(x+\mu)((x+\mu)^2+y^2)^2}{\|(\mathbf{r}_1\times\hat{\mathbf{z}})\times\mathbf{r}_1\|_2^3}\bigg) \end{aligned} \tag{D.3}$$

$$\begin{aligned} a_{2,yx} =&\beta\frac{(1-\mu)d_2^2\rho p(\phi)}{r_2^4}\cos^2(\psi-\alpha)\bigg(-\frac{4(x-1+\mu)n_y}{r_2^2} \\ &-\frac{\cos\alpha(x+\mu)y}{r_1^3}-\frac{\sin\alpha\sin\gamma y^2}{\|\mathbf{r}_1\times\hat{\mathbf{z}}\|_2^3} \\ &+\frac{\sin\alpha\cos\gamma(x+\mu)yz(2(x+\mu)^2+2y^2+z^2)}{\|(\mathbf{r}_1\times\hat{\mathbf{z}})\times\mathbf{r}_1\|_2^3}\bigg) \end{aligned} \tag{D.4}$$

$$
\begin{aligned}
a_{2,yy} =&\beta\frac{(1-\mu)d_2^2\rho p(\phi)}{r_2^4}\cos^2(\psi-\alpha)\bigg(-\frac{4yn_y}{r_2^2}\\
&+\frac{\cos\alpha((x+\mu)^2+z^2)}{r_1^3}+\frac{\sin\alpha\sin\gamma y^2}{\|\mathbf{r}_1\times\hat{\mathbf{z}}\|_2^3}\\
&-\frac{\sin\alpha\cos\gamma z((x+\mu)^2(z^2+(x+\mu)^2)-y^4)}{\|(\mathbf{r}_1\times\hat{\mathbf{z}})\times\mathbf{r}_1\|_2^3}\bigg) \qquad \text{(D.5)}\\
a_{2,yz} =&\beta\frac{(1-\mu)d_2^2\rho p(\phi)}{r_2^4}\cos^2(\psi-\alpha)\bigg(-\frac{4zn_y}{r_2^2}-\frac{\cos\alpha zy}{r_1^3}\\
&-\frac{\sin\alpha\cos\gamma y((x+\mu)^2+y^2)^2}{\|(\mathbf{r}_1\times\hat{\mathbf{z}})\times\mathbf{r}_1\|_2^3}\bigg) \qquad \text{(D.6)}\\
a_{2,zx} =&\beta\frac{(1-\mu)d_2^2\rho p(\phi)}{r_2^4}\cos^2(\psi-\alpha)\bigg(-\frac{4(x-1+\mu)n_z}{r_2^2}\\
&-\frac{\cos\alpha(x+\mu)z}{r_1^3}+\frac{\sin\alpha\cos\gamma(x+\mu)z^2((x+\mu)^2+y^2)}{\|(\mathbf{r}_1\times\hat{\mathbf{z}})\times\mathbf{r}_1\|_2^3}\bigg) \qquad \text{(D.7)}\\
a_{2,zy} =&\beta\frac{(1-\mu)d_2^2\rho p(\phi)}{r_2^4}\cos^2(\psi-\alpha)\bigg(-\frac{4yn_z}{r_2^2}-\frac{\cos\alpha yz}{r_1^3}\\
&+\frac{\sin\alpha\cos\gamma yz^2((x+\mu)^2+y^2)}{\|(\mathbf{r}_1\times\hat{\mathbf{z}})\times\mathbf{r}_1\|_2^3}\bigg) \qquad \text{(D.8)}\\
a_{2,zz} =&\beta\frac{(1-\mu)d_2^2\rho p(\phi)}{r_2^4}\cos^2(\psi-\alpha)\bigg(-\frac{4zn_z}{r_2^2}\\
&+\frac{\cos\alpha((x+\mu)^2+y^2)}{r_1^3}-\frac{\sin\alpha\cos\gamma z((x+\mu)^2+y^2)^2}{\|(\mathbf{r}_1\times\hat{\mathbf{z}})\times\mathbf{r}_1\|_2^3}\bigg) \qquad \text{(D.9)}
\end{aligned}
$$

Appendix E. Partial Derivatives of the Solar Sail SRP Acceleration Terms Relative to Orientation

The scalar expressions for the second partial derivatives of the solar sail acceleration $\mathbf{a}_1$ with respect to orientation are expressed given here.

$$a_{1,x\alpha} = \beta\frac{(1-\mu)}{r_1^2}\cos\alpha\bigg(-\frac{3\cos\alpha\sin\alpha(x+\mu)}{r_1}+\frac{(1-3\sin^2\alpha)\sin\gamma y}{\|\mathbf{r}_1\times\hat{\mathbf{z}}\|_2} - \frac{(1-3\sin^2\alpha)\cos\gamma(x+\mu)z}{\|(\mathbf{r}_1\times\hat{\mathbf{z}})\times\mathbf{r}_1\|_2}\bigg) \tag{E.1}$$

$$a_{1,y\alpha} = \beta\frac{(1-\mu)}{r_1^2}\cos\alpha\bigg(-\frac{3\cos\alpha\sin\alpha y}{r_1}-\frac{(1-3\sin^2\alpha)\sin\gamma(x+\mu)}{\|\mathbf{r}_1\times\hat{\mathbf{z}}\|_2} - \frac{(1-3\sin^2\alpha)\cos\gamma yz}{\|(\mathbf{r}_1\times\hat{\mathbf{z}})\times\mathbf{r}_1\|_2}\bigg) \tag{E.2}$$

$$a_{1,z\alpha} = \beta\frac{(1-\mu)}{r_1^2}\cos\alpha\bigg(-\frac{3\cos\alpha\sin\alpha z}{r_1} - \frac{(1-3\sin^2\alpha)\cos\gamma(y^2+(x+\mu)^2)}{\|(\mathbf{r}_1\times\hat{\mathbf{z}})\times\mathbf{r}_1\|_2}\bigg) \tag{E.3}$$

$$a_{1,x\gamma} = \beta\frac{(1-\mu)}{r_1^2}\cos^2\alpha\bigg(\frac{\sin\alpha\cos\gamma y}{\|\mathbf{r}_1\times\hat{\mathbf{z}}\|_2}+\frac{\sin\alpha\sin\gamma(x+\mu)z}{\|(\mathbf{r}_1\times\hat{\mathbf{z}})\times\mathbf{r}_1\|_2}\bigg) \tag{E.4}$$

$$a_{1,y\gamma} = \beta\frac{(1-\mu)}{r_1^2}\cos^2\alpha\bigg(-\frac{\sin\alpha\cos\gamma(x+\mu)}{\|\mathbf{r}_1\times\hat{\mathbf{z}}\|_2}+\frac{\sin\alpha\sin\gamma yz}{\|(\mathbf{r}_1\times\hat{\mathbf{z}})\times\mathbf{r}_1\|_2}\bigg) \tag{E.5}$$

$$a_{1,z\gamma} = \beta\frac{(1-\mu)}{r_1^2}\cos^2\alpha\bigg(-\frac{\sin\alpha\sin\gamma(y^2+(x+\mu)^2)}{\|(\mathbf{r}_1\times\hat{\mathbf{z}})\times\mathbf{r}_1\|_2}\bigg) \tag{E.6}$$

Appendix F. Partial Derivatives of the Solar Sail ARP Acceleration Terms Relative to Orientation

The scalar expressions for the second partial derivatives of the solar sail acceleration $\mathbf{a}_2$ with respect to orientation are given here.

$$\begin{aligned} a_{2,x\alpha} =&\beta\frac{(1-\mu)d_2^2\rho p(\phi)}{r_2^4}\cos(\psi-\alpha) \\ &\left(\frac{(2\sin(\psi-\alpha)\cos\alpha-\cos(\psi-\alpha)\sin\alpha)\,(x+\mu)}{r_1}\right. \\ &+\frac{(2\sin(\psi-\alpha)\sin\alpha+\cos(\psi-\alpha)\cos\alpha)\sin\gamma y}{\|\mathbf{r}_1\times\hat{\mathbf{z}}\|_2} \\ &\left.-\frac{(2\sin(\psi-\alpha)\sin\alpha+\cos(\psi-\alpha)\cos\alpha)\cos\gamma(x+\mu)z}{\|(\mathbf{r}_1\times\hat{\mathbf{z}})\times\mathbf{r}_1\|_2}\right) \end{aligned} \tag{F.1}$$

$$\begin{aligned} a_{2,y\alpha} =&\beta\frac{(1-\mu)d_2^2\rho p(\phi)}{r_2^4}\cos(\psi-\alpha) \\ &\left(\frac{(2\sin(\psi-\alpha)\cos\alpha-\cos(\psi-\alpha)\sin\alpha)\,y}{r_1}\right. \\ &-\frac{(2\sin(\psi-\alpha)\sin\alpha+\cos(\psi-\alpha)\cos\alpha)\sin\gamma(x+\mu)}{\|\mathbf{r}_1\times\hat{\mathbf{z}}\|_2} \\ &\left.-\frac{(2\sin(\psi-\alpha)\sin\alpha+\cos(\psi-\alpha)\cos\alpha)\,yz}{\|(\mathbf{r}_1\times\hat{\mathbf{z}})\times\mathbf{r}_1\|_2}\right) \end{aligned} \tag{F.2}$$

$$\begin{aligned} a_{2,z\alpha} =&\beta\frac{(1-\mu)d_2^2\rho p(\phi)}{r_2^4}\cos(\psi-\alpha) \\ &\left(\frac{(2\sin(\psi-\alpha)\cos\alpha-\cos(\psi-\alpha)\sin\alpha)\,z}{r_1}\right. \\ &\left.-\frac{(2\sin(\psi-\alpha)\sin\alpha+\cos(\psi-\alpha)\cos\alpha)\cos\gamma(y^2+(x+\mu)^2)}{\|(\mathbf{r}_1\times\hat{\mathbf{z}})\times\mathbf{r}_1\|_2}\right) \end{aligned} \tag{F.3}$$

$$\begin{aligned} a_{2,x\gamma} =&\beta\frac{(1-\mu)d_2^2\rho p(\phi)}{r_2^4}\cos^2(\psi-\alpha)\left(\frac{\sin\alpha\cos\gamma y}{\|\mathbf{r}_1\times\hat{\mathbf{z}}\|_2}\right. \\ &\left.+\frac{\sin\alpha\sin\gamma(x+\mu)z}{\|(\mathbf{r}_1\times\hat{\mathbf{z}})\times\mathbf{r}_1\|_2}\right) \end{aligned} \tag{F.4}$$

$$a_{2,y\gamma} = \beta \frac{\beta(1-\mu) d_2^2 \rho p(\phi)}{r_2^4} \cos^2(\psi - \alpha) \Bigg(- \frac{\sin\alpha \cos\gamma (x+\mu)}{\|\mathbf{r}_1 \times \hat{\mathbf{z}}\|_2} + \frac{\sin\alpha \sin\gamma yz}{\|(\mathbf{r}_1 \times \hat{\mathbf{z}}) \times \mathbf{r}_1\|_2} \Bigg) \tag{F.5}$$

$$a_{2,z\gamma} = \beta \frac{(1-\mu) d_2^2 \rho p(\phi)}{r_2^4} \cos^2(\psi - \alpha) \Bigg(- \frac{\sin\alpha \sin\gamma (y^2 + (x+\mu)^2)}{\|(\mathbf{r}_1 \times \hat{\mathbf{z}}) \times \mathbf{r}_1\|_2} \Bigg) \tag{F.6}$$

Appendix G. Derivation of Partial Derivatives of the SRP and ARP Acceleration Terms Relative to Orientation

This section shows how the equations were derived in Appendix E and Appendix F. Derivation of $a_{1,x}$ and $a_{2,x}$ with respect to each orientation angle is shown.

$$
\begin{aligned}
a_{1,x\alpha} =& \frac{\partial}{\partial\alpha}\beta\frac{(1-\mu)}{r_1^2}\cos^2\alpha n_x \\
=& \frac{\partial}{\partial\alpha}\beta\frac{(1-\mu)}{r_1^2}\cos^2\alpha\left(\frac{\cos\alpha(x+\mu)}{r_1} - \frac{\sin\alpha\cos\gamma(x+\mu)z}{\|(\mathbf{r}_1\times\hat{\mathbf{z}})\times\mathbf{r}_1\|_2} + \frac{\sin\alpha\sin\gamma y}{\|\mathbf{r}_1\times\hat{\mathbf{z}}\|_2}\right) \\
=& \beta\frac{(1-\mu)}{r_1^2}\left(-2\cos\alpha\sin\alpha\left(\frac{\cos\alpha(x+\mu)}{r_1} - \frac{\sin\alpha\cos\gamma(x+\mu)z}{\|(\mathbf{r}_1\times\hat{\mathbf{z}})\times\mathbf{r}_1\|_2}\right.\right. \\
&\left. + \frac{\sin\alpha\sin\gamma y}{\|\mathbf{r}_1\times\hat{\mathbf{z}}\|_2}\right) + \cos^2\alpha\left(-\frac{\sin\alpha(x+\mu)}{r_1} - \frac{\cos\alpha\cos\gamma(x+\mu)z}{\|(\mathbf{r}_1\times\hat{\mathbf{z}})\times\mathbf{r}_1\|_2}\right. \\
&\left.\left. + \frac{\cos\alpha\sin\gamma y}{\|\mathbf{r}_1\times\hat{\mathbf{z}}\|_2}\right)\right) \\
=& \beta\frac{(1-\mu)}{r_1^2}\left(-\frac{2\cos^2\alpha\sin\alpha(x+\mu)}{r_1} + \frac{2\cos\alpha\sin^2\alpha\cos\gamma(x+\mu)z}{\|(\mathbf{r}_1\times\hat{\mathbf{z}})\times\mathbf{r}_1\|_2}\right. \\
&- \frac{2\cos\alpha\sin^2\alpha\sin\gamma y}{\|\mathbf{r}_1\times\hat{\mathbf{z}}\|_2} - \frac{\cos^2\alpha\sin\alpha(x+\mu)}{r_1} - \frac{\cos^3\alpha\cos\gamma(x+\mu)z}{\|(\mathbf{r}_1\times\hat{\mathbf{z}})\times\mathbf{r}_1\|_2} \\
&\left. + \frac{\cos^3\alpha\sin\gamma y}{\|\mathbf{r}_1\times\hat{\mathbf{z}}\|_2}\right)
\end{aligned}
$$

$$
\begin{aligned}
=&\beta\frac{(1-\mu)}{r_1^2}\cos\alpha\Bigg(-\frac{2\cos\alpha\sin\alpha(x+\mu)}{r_1}+\frac{2\sin^2\alpha\cos\gamma(x+\mu)z}{\|(\mathbf{r}_1\times\hat{\mathbf{z}})\times\mathbf{r}_1\|_2}\\
&-\frac{2\sin^2\alpha\sin\gamma y}{\|\mathbf{r}_1\times\hat{\mathbf{z}}\|_2}-\frac{\cos\alpha\sin\alpha(x+\mu)}{r_1}-\frac{\cos^2\alpha\cos\gamma(x+\mu)z}{\|(\mathbf{r}_1\times\hat{\mathbf{z}})\times\mathbf{r}_1\|_2}\\
&+\frac{\cos^2\alpha\sin\gamma y}{\|\mathbf{r}_1\times\hat{\mathbf{z}}\|_2}\Bigg)\\
=&\beta\frac{(1-\mu)}{r_1^2}\cos\alpha\Bigg(-\frac{3\cos\alpha\sin\alpha(x+\mu)}{r_1}\\
&-\frac{(-2\sin^2\alpha+\cos^2\alpha)\cos\gamma(x+\mu)z}{\|(\mathbf{r}_1\times\hat{\mathbf{z}})\times\mathbf{r}_1\|_2}+\frac{(-2\sin^2\alpha+\cos^2\alpha)\sin\gamma y}{\|\mathbf{r}_1\times\hat{\mathbf{z}}\|_2}\Bigg)\\
=&\beta\frac{(1-\mu)}{r_1^2}\cos\alpha\Bigg(-\frac{3\cos\alpha\sin\alpha(x+\mu)}{r_1}\\
&-\frac{(-2\sin^2\alpha+1-\sin^2\alpha)\cos\gamma(x+\mu)z}{\|(\mathbf{r}_1\times\hat{\mathbf{z}})\times\mathbf{r}_1\|_2}\\
&+\frac{(-2\sin^2\alpha+1-\sin^2\alpha)\sin\gamma y}{\|\mathbf{r}_1\times\hat{\mathbf{z}}\|_2}\Bigg)\\
=&\beta\frac{(1-\mu)}{r_1^2}\cos\alpha\Bigg(-\frac{3\cos\alpha\sin\alpha(x+\mu)}{r_1}+\frac{(1-3\sin^2\alpha)\sin\gamma y}{\|\mathbf{r}_1\times\hat{\mathbf{z}}\|_2}\\
&-\frac{(1-3\sin^2\alpha)\cos\gamma(x+\mu)z}{\|(\mathbf{r}_1\times\hat{\mathbf{z}})\times\mathbf{r}_1\|_2}\Bigg) \qquad \text{(G.1)}\\
a_{1,x\gamma}=&\frac{\partial}{\partial\gamma}\beta\frac{(1-\mu)}{r_1^2}\cos^2\alpha n_x\\
=&\frac{\partial}{\partial\gamma}\beta\frac{(1-\mu)}{r_1^2}\cos^2\alpha\Bigg(\frac{\cos\alpha(x+\mu)}{r_1}-\frac{\sin\alpha\cos\gamma(x+\mu)z}{\|(\mathbf{r}_1\times\hat{\mathbf{z}})\times\mathbf{r}_1\|_2}+\\
&\frac{\sin\alpha\sin\gamma y}{\|\mathbf{r}_1\times\hat{\mathbf{z}}\|_2}\Bigg)\\
=&\beta\frac{(1-\mu)}{r_1^2}\cos^2\alpha\Bigg(\frac{\sin\alpha\cos\gamma y}{\|\mathbf{r}_1\times\hat{\mathbf{z}}\|_2}+\frac{\sin\alpha\sin\gamma(x+\mu)z}{\|(\mathbf{r}_1\times\hat{\mathbf{z}})\times\mathbf{r}_1\|_2}\Bigg) \qquad \text{(G.2)}
\end{aligned}
$$

$$
\begin{aligned}
a_{2,x\alpha} =& \frac{\partial}{\partial \alpha} \beta \frac{(1-\mu) d_2^2 \rho p(\phi)}{r_2^4} \cos^2(\psi - \alpha) n_x \\
=& \frac{\partial}{\partial \alpha} \beta \frac{(1-\mu) d_2^2 \rho p(\phi)}{r_2^4} \cos^2(\psi - \alpha) \Bigg(\frac{\cos\alpha (x+\mu)}{r_1} \\
& - \frac{\sin\alpha \cos\gamma (x+\mu) z}{\| (\mathbf{r}_1 \times \hat{\mathbf{z}}) \times \mathbf{r}_1 \|_2} + \frac{\sin\alpha \sin\gamma y}{\| \mathbf{r}_1 \times \hat{\mathbf{z}} \|_2} \Bigg) \\
=& \beta \frac{(1-\mu) d_2^2 \rho p(\phi)}{r_2^4} \Bigg(2\cos(\psi - \alpha) \sin(\psi - \alpha) \Bigg(\frac{\cos\alpha (x+\mu)}{r_1} \\
& - \frac{\sin\alpha \cos\gamma (x+\mu) z}{\| (\mathbf{r}_1 \times \hat{\mathbf{z}}) \times \mathbf{r}_1 \|_2} + \frac{\sin\alpha \sin\gamma y}{\| \mathbf{r}_1 \times \hat{\mathbf{z}} \|_2} \Bigg) \\
& + \cos^2(\psi - \alpha) \Bigg(- \frac{\sin\alpha (x+\mu)}{r_1} - \frac{\cos\alpha \cos\gamma (x+\mu) z}{\| (\mathbf{r}_1 \times \hat{\mathbf{z}}) \times \mathbf{r}_1 \|_2} \\
& + \frac{\cos\alpha \sin\gamma y}{\| \mathbf{r}_1 \times \hat{\mathbf{z}} \|_2} \Bigg) \Bigg) \\
=& \beta \frac{(1-\mu) d_2^2 \rho p(\phi)}{r_2^4} \cos(\psi - \alpha) \\
& \Bigg(\frac{(2\sin(\psi - \alpha)\cos\alpha - \cos(\psi - \alpha)\sin\alpha)(x+\mu)}{r_1} \\
& + \frac{(2\sin(\psi - \alpha)\sin\alpha + \cos(\psi - \alpha)\cos\alpha)\sin\gamma y}{\| \mathbf{r}_1 \times \hat{\mathbf{z}} \|_2} \\
& - \frac{(2\sin(\psi - \alpha)\sin\alpha + \cos(\psi - \alpha)\cos\alpha)\cos\gamma (x+\mu) z}{\| (\mathbf{r}_1 \times \hat{\mathbf{z}}) \times \mathbf{r}_1 \|_2} \Bigg)
\end{aligned} \tag{G.3}
$$

$$
\begin{aligned}
a_{2,x\gamma} =& \frac{\partial}{\partial \gamma} \beta \frac{(1-\mu) d_2^2 \rho p(\phi)}{r_2^4} \cos^2(\psi - \alpha) n_x \\
=& \frac{\partial}{\partial \gamma} \beta \frac{(1-\mu) d_2^2 \rho p(\phi)}{r_2^4} \cos^2(\psi - \alpha) \\
& \Bigg(\frac{\cos\alpha (x+\mu)}{r_1} - \frac{\sin\alpha \cos\gamma (x+\mu) z}{\| (\mathbf{r}_1 \times \hat{\mathbf{z}}) \times \mathbf{r}_1 \|_2} + \frac{\sin\alpha \sin\gamma y}{\| \mathbf{r}_1 \times \hat{\mathbf{z}} \|_2} \Bigg) \\
=& \beta \frac{(1-\mu) d_2^2 \rho p(\phi)}{r_2^4} \cos^2(\psi - \alpha) \Bigg(\frac{\sin\alpha \cos\gamma y}{\| \mathbf{r}_1 \times \hat{\mathbf{z}} \|_2} \\
& + \frac{\sin\alpha \sin\gamma (x+\mu) z}{\| (\mathbf{r}_1 \times \hat{\mathbf{z}}) \times \mathbf{r}_1 \|_2} \Bigg)
\end{aligned} \tag{G.4}
$$